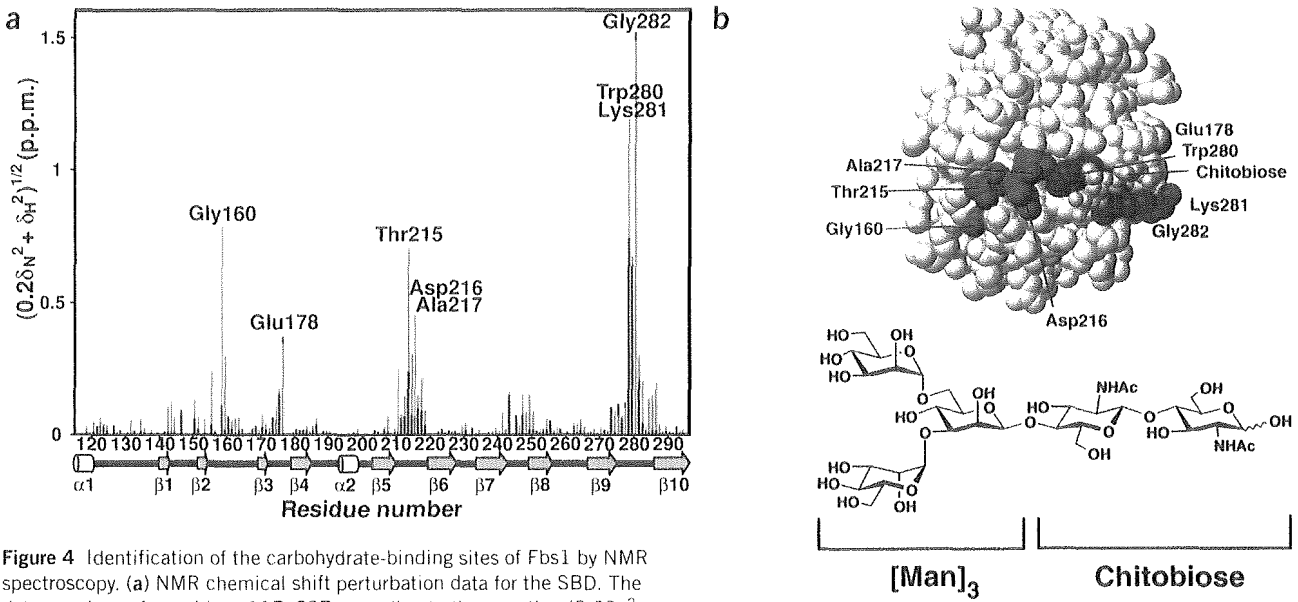

Figure 4 Identification of the carbohydrate-binding sites of Fbs1 by NMR spectroscopy. (**a**) NMR chemical shift perturbation data for the SBD. The data are shown for residues 117–297 according to the equation $(0.2\delta_N^2 + \delta_H^2)^{1/2}$, where δ_N and δ_H represent the change in nitrogen and proton chemical shifts on addition of chitobiose (blue) and $Man_3GlcNAc_2$ (red). Secondary structure elements for SBD are shown below the plot. (**b**) Mapping the perturbed residues of the SBD(97–297) ($(0.2\delta_N^2 + \delta_H^2)^{1/2} > 0.3$) upon binding to chitobiose (blue) and $Man_3GlcNAc_2$ (blue and red). The chitobiose molecule bound to SBD is yellow. The $Man_3GlcNAc_2$ structure is represented in the right panel.

mannose branches to the interaction with Fbs1, because it is generally not feasible to crystallize or to interpret the electron density of complexes of lectins with larger oligosaccharides. To identify the oligosaccharide-binding site of the SBD in solution, we compared the pattern of the chemical shift perturbation between chitobiose and$Man_3GlcNAc_2$ (Manα1→3[Manα1→6]Manβ1→4GlcNAcβ1→4GlcNAc) using the isotopically labeled SBD (**Fig. 4** and see **Supplementary Fig. 1** online). Chitobiose binding resulted in marked chemical shift perturbation for Glu178 in the L1 loop and for Trp280, Lys281 and Gly282 in the L2 loop; this is consistent with the X-ray structure of the C132A SBD–chitobiose complex. When $Man_3GlcNAc_2$ was used as a ligand, chemical shift perturbations were observed for Gly160, Thr215, Asp216 and Ala217 in addition to the residues perturbed by chitobiose, indicating that the outer branches of the carbohydrate moiety interact with the β5–β6 loop. In the crystal structure of the SBD–chitobiose complex, O4 of GlcNAc(A) is oriented toward these amino acid residues. Thus, the orientation of the sugar chain deduced from the NMR data is consistent with the expected orientation on inspection of the crystal structure. Although mannose residues of $Man_3GlcNAc_2$ seem to interact with the β5–β6 loop of Fbs1, almost no chemical shift perturbation of any consequence was observed upon addition of mannotriose (Manα1→3[Manα1→6]Man) alone (data not shown), suggesting that the affinity of $Man_3GlcNAc_2$ is dominated by the interaction with its chitobiose portion.

DISCUSSION

In the present study, we determined the SBD structure of Fbs1 and its complex with chitobiose. In general, most lectins bind nonreducing terminal sugar groups in the concave surface, which consists of several strands of β-sheets. The substrate-binding site of galectin-3 that forms a complex with *N*-acetyl-lactosamine is formed by β-strands[18]. The amino acids in these β-strands interact with the bound substrate through direct and water-mediated hydrogen bonds or through van der Waals contacts. In contrast, Fbs1 recognizes the inner chitobiose of N-linked high-mannose oligosaccharides by a specific binding surface located at one tip of the β-sandwich. To our knowledge, this is the first report of the sugar-binding mode of lectins, that is, interaction with the innermost portion of the carbohydrate moieties of glycoproteins. This is in marked contrast to the lectin chaperones in the ER, namely calnexin and calreticulin, which recognize nonreducing terminal glucose molecules of the high-mannose oligosaccharides expressed on their target glycoproteins.

In crystal structures of glycoproteins, electron densities of carbohydrate moieties are generally ambiguous because the carbohydrate moieties attached to the crystallized proteins do not necessarily exhibit a uniform chemical structure and may possess freedom of internal motion. In many cases, however, the innermost GlcNAc residue does provide unambiguous electron density because it is involved in interactions with the polypeptide moieties. It seems that those intramolecular interactions hamper the binding of Fbs1 to the chitobiose portions of glycoproteins as a result of steric hindrance in their native states. We propose that the novel sugar-binding mode embodied by Fbs1 is suitable for recognition of unfolded glycoproteins targeted in the ERAD system. RNase B used in the *in vitro* binding assay reveals an oligosaccharide that does not contact the polypeptide chain except at the covalent attachment point[23]. This glycoprotein could interact with Fbs1 even in the native form in the *in vitro* binding experiment, probably as a result of the exceptional freedom of the chitobiose portion of its carbohydrate moiety.

On inspection of the X-ray crystallographic and mutagenesis data, we conclude that the hydrophobic interaction between the GlcNAc(A) residue and Trp280, the hydrophobic interaction between the GlcNAc(B) residue and the small hydrophobic pocket composed of Phe177 and Tyr279, and the hydrogen bonds between the chitobiose and Fbs1 atoms, are essential for selective binding to this disaccharide moiety. Recently, we reported that Fbs2 also binds high-mannose oligosaccharides in a chitobiose-dependent manner, but the strength

Table 1 Data collection, phasing and refinement statistics

Data collection

	Native	PCMBS	$NaAuCl_4$	$SmCl_3$	$OsCl_3$	$HgNO_3$	Complex
Space group	$P3_221$						$P4_32_12$
Resolution (Å)	2.0	2.5	2.7	2.5	2.7	2.2	2.4
Observations	192,305	100,271	80,395	59,131	79,742	96,045	93,981
Unique reflections	18,483	9,577	7,689	9,633	7,695	13,725	12,611
Completeness (%)[a]	99.9 (99.9)	99.8 (99.8)	99.8 (99.8)	99.8 (99.8)	99.8 (99.8)	98.6 (98.6)	99.8 (99.8)
Redundancy[a]	10.4 (10.1)	10.5 (10.6)	10.5 (10.6)	6.1 (6.2)	10.4 (10.5)	7.0 (6.9)	7.5 (7.2)
R_{sym} (%)[a,b]	9.5 (27.8)	12.5 (30.6)	9.9 (24.0)	13.5 (22.7)	14.3 (28.0)	14.4 (26.4)	8.5 (18.4)
I / σ[a]	4.4 (2.5)	4.4 (2.3)	6.0 (2.9)	3.9 (3.0)	3.7 (2.3)	3.2 (2.6)	6.4 (3.6)

MIRAS phasing

Resolution (Å)	2.5	2.7	2.5	2.7	2.2		
Heavy atom sites	3	2	2	1	2		
Phasing power	1.37	0.89	0.76	1.71	3.31		
R_{cullis}[c]	0.8	0.84	0.88	0.69	0.46		

Refinement statistics

	SBD	SBD C132A–chitobiose
Resolution (Å)	2.0	2.4
Reflections	17,470	11,950
Total atoms	1,602	1,562
R-factor (%)	16.2	20.0
R_{free} (%)	19.9	26.3
R.m.s. deviations		
Bond length (Å)	0.020	0.038
Bond angle (°)	1.8	2.9

[a]Values in parentheses are for the highest-resolution shell. [b]$R_{sym} = \Sigma_h \Sigma_j |I_{hj} - \langle I_h \rangle| / \Sigma_h \Sigma_j |I_{hj}|$, where h represents a unique reflection and j represents symmetry-equivalent indices. I is the observed intensity and $\langle I \rangle$ is the mean value of I. [c]$R_{cullis} = \Sigma ||F_{PH}| \pm |F_P|| - |F_H|| / \Sigma |F_{PH}| \pm |F_P|$.

of the glycoprotein-binding ability is weaker than that of Fbs1 (ref. 8). In Fbs2, the positions corresponding to Phe177, Tyr279 and Trp280 in Fbs1 are occupied by phenylalanine, phenylalanine, and tryptophan, respectively (Fig. 1c). The conservation of these residues suggests that the chitobiose-binding mode of Fbs2 is similar to that of Fbs1, and the reduced binding ability of Fbs2 may be attributed to the Tyr→Phe substitution in the chitobiose-binding pocket. Fbs1 interacts not only with chitobiose at the L1 and L2 loops but also with the outer mannose residues at the β5–β6 loop. Although binding of mannose residues to the β5–β6 loop seems to strengthen the binding affinity, mannose did not bind alone. This inner chitobiose-dependent interaction mode further restricts Fbs1 to interacting with native proteins carrying high-mannose oligosaccharides. The positions corresponding to Thr215 and Ala217, which are involved in the interaction with the mannose residues, are occupied by alanine and cysteine, respectively, in Fbs2 (Fig. 1c). This might be associated with the distinct affinity of Fbs1 and Fbs2 to N-glycans (ref. 8).

We attempted to model the full-length Fbs1 protein and its assembly in the SCF-E2 complex by positioning the N terminus of the SBD adjacent to the F-box domain of the reported SCF^{Skp2} complex[9]. This model places the chitobiose >50 Å from the expected position of the E2 protein that donates ubiquitin to the glycoprotein, consistent with modeling of other SCF complexes, such as SCF^{Skp2} (ref. 9) and SCF^{Cdc4} (ref. 11).

Fbs1 is a functionally unique molecule that recognizes the innermost position of N-glycans as a signal for denatured glycoproteins. Our results confirmed structurally that N-glycans act as a ubiquitination signal, thus providing new insights into the biological roles of sugar chains coupled to proteins within cells.

METHODS

Crystallization and structure determination. The SBD of murine Fbs1(117–297), with a molecular mass of 20.6 kDa, and its mutant protein C132A SBD were cloned into pET15b and expressed in *Escherichia coli*. Both proteins were purified by nickel affinity and gel filtration chromatography and concentrated to 20 mg ml^{-1}. All mutations were constructed by QuikChange mutagenesis kit (Stratagene), using synthetic oligonucleotides, and the sequences were verified in their entirety.

Crystals of SBD were grown at 25 °C by the hanging-drop vapor diffusion method. SBD crystals were grown from 1.7 M ammonium sulfate, 0.01 M nickel chloride, 0.1% (v/v) PEG400 and 0.1 M Tris-HCl, pH 8.5. The C132A SBD was cocrystallized with chitobiose (Seikagaku). C132A SBD crystals were prepared using 1.4 M sodium chloride, 1.7 M ammonium sulfate, 0.1 M PIPES, pH 7.0, and 30 mM chitobiose. SBD and its cysteine mutant crystals belonged to $P3_221$ and $P4_32_12$ space groups, with cell dimensions of $a = b = 62.4$ Å, $c = 117.2$ Å, and $a = b = 63.8$ Å, $c = 147.8$ Å, respectively. Heavy-atom soaks were done in crystallization buffer with saturated *p*-chloromercuribenzene sulfonate (PCMBS) (for 3 h), 10 mM $NaAuCl_4$ (15 h), 10 mM $SmCl_3$ (15 h), 10 mM $OsCl_3$ (15 h) and 10 mM $HgNO_3$ (15 h). Intensity data sets were collected on a Rigaku R-AXIS IV nickel-filtered double-mirror focused CuKα-radiation detector. A Rigaku RU-200 rotating-anode X-ray generator was operated at 40 kV and 100 mA. Data were processed with MOSFLM[24] and SCALA[25,26]. The structure of the SBD was determined by the multiple isomorphous replacement anomalous scattering (MIRAS) method. Phases were calculated with MLPHARE[26] to 2.2 Å. The initial electron density map was then refined by solvent flattening[27] and histogram mapping[28] using DM[26]. The initial model was constructed with Arp/WArp[29] and O[30]. The model was refined at a resolution of 2.0 Å with REFMAC[31]. Residues 43–55 of the SBD have high temperature factors and are presumably partially disordered.

Intensity data sets of the mutant protein were collected at 100 K. For cryoprotection, 20% (v/v) glycerol was added to the crystallizing solution. The

structure of C132A was determined by the molecular replacement technique using AMoRe[32] with the refined model of SBD. Structure refinement of the mutant SBD was guided by referring to the structure of the wild type. Refinement statistics of both structures are summarized in Table 1.

Binding assay. Neuro2a cells were transfected with Flag-tagged murine Fbs1 ΔN-2(95–297) and its derivatives that lack the region from the N terminus to the F-box domain[7] by lipofection (Lipofectamine Plus; Gibco BRL). At 48 h after transfection, the whole-cell extracts (WCEs), solubilized with TBS containing 0.5% (v/v) NP-40, were used for immunoprecipitation using mouse monoclonal anti-Flag (M2; Sigma), or pull-down assay using RNase B–immobilized resin, as described[7]. The (co-)immunoprecipitated proteins were detected by immunoblotting using mouse monoclonal antibodies anti-Flag (M2) and anti-integrin β1 (Transduction Laboratories).

***In vitro* ubiquitination assay.** Recombinant His-tagged human Ubc4 was produced in *E. coli*. Recombinant His-tagged mouse E1 (Uba1), His-tagged rat Fbs1 (ΔN-2) and each SCF^{Fbs1} (Flag-tagged human Skp1, human Cul1-HA/His-tagged rat Fbs1 derivatives, T7-tagged human Roc1) were produced by baculovirus-infected HiFive insect cells. Each SCF^{Fbs1} complex was obtained by simultaneously infecting four baculoviruses. These proteins were affinity-purified by a HiTrap HP column (Amersham Pharmacia Biotech), as described[7]. Each 1 μg of GTF was incubated in 50 μl of the reaction mixture containing ATP-regenerating system, 0.5 μg E1, 1 μg Ubc4 (E2), 2 μg SCF^{Fbs1}, 6.5 μg recombinant GST-ubiquitin and NEDD8 system[33] at 30 °C. After the reaction was terminated by adding 25 μl of 3× SDS-PAGE sample buffer, the proteins in 8 μl of the boiled supernatants were separated with 5–20% (w/v) SDS-PAGE, and the high-molecular-mass ubiquitinated proteins were detected by immunoblotting with anti-fetuin (Chemicon International).

NMR spectroscopy. The DNA fragment encoding residues 97–297 of Fbs1was inserted into the pGEX-6P-1 plasmid vector (Amersham Biosciences) with a N-terminal GST moiety. The protein was expressed in *E. coli* BL21(DE3) CodonPlus strain (Stratagene) in M9 minimal medium with appropriate [^{15}N]NH_4Cl and [$^{13}C_6$]glucose. GST-fusion protein was purified from cell lysates on a glutathione-Sepharose column. The fusion protein was cleaved by incubation with PreScission protease (Amersham Biosciences), and GST was removed by loading a second glutathione-Sepharose column. The protein was further purified using a Superose12 gel filtration column.

NMR samples contained 0.1–1.0 mM SBD(97–297) in 10 mM NaH_2PO_4/Na_2HPO_4, pH 6.5, 50 mM KCl and 10 mM DTT. For chemical shift perturbation experiments, a ten-fold molar excess of chitobiose, ten-fold molar excess of Manα1′3(Manα1′6)Man (Calbiochem) or one molar equivalent of $Man_3GlcNAc_2$ (Sigma) was added to the protein solution. NMR spectra were acquired at 30 °C on Bruker DMX500 and DRX800 spectrometers. The ^{1}H, ^{15}N and ^{13}C resonances of the backbone were assigned using a standard set of double- and triple-resonance experiments[34].

Coordinates. The atomic coordinates of the SBD and C132A SBD–chitobiose complex have been deposited in the Protein Data Bank (accession codes 1UMH and 1UMI, respectively).

Note: Supplementary information is available on the Nature Structural & Molecular Biology website.

ACKNOWLEDGMENTS

We thank Y. Wada for her help in the preparation of isotopically labeled recombinant proteins and E. Adachi for expert technical assistance. This work was supported in part by Grants-in-Aid from the Ministry of Education, Science and Culture of Japan (K.T. and K.K.), Japan Society for the Promotion of Science and Mizutani Foundation for Glycoscience (K.K.), and in part by the National Project on Protein Structural and Functional Analyses from the Ministry of Education, Culture, Sport, Science and Technology of Japan (T.T.).

COMPETING INTERESTS STATEMENT

The authors declare that they have no competing financial interests.

Received 6 October 2003; accepted 20 January 2004
Published online at http://www.nature.com/natstructmolbiol/

1. Hershko, A., Ciechanover, A. & Varshavsky, A. Basic Medical Research Award. The ubiquitin system. *Nat. Med.* **6**, 1073–1081 (2000).
2. Pickart, C.M. Mechanisms underlying ubiquitination. *Annu. Rev. Biochem.* **70**, 503–533 (2001).
3. Weissman, A.M. Themes and variations on ubiquitylation. *Nat. Rev. Mol. Cell. Biol.* **2**, 169–178 (2001).
4. Deshaies, R.J. SCF and Cullin/Ring H2–based ubiquitin ligases. *Annu. Rev. Cell. Dev. Biol.* **15**, 435–467 (1999).
5. Winston, J.T., Koepp, D.M., Zhu, C., Elledge, S.J. & Harper, J.W. A family of mammalian F-box proteins. *Curr. Biol.* **9**, 1180–1182 (1999).
6. Ilyin, G.P. *et al.* A new subfamily of structurally related human F-box proteins. *Gene* **296**, 11–20 (2002).
7. Yoshida, Y. *et al.* E3 ubiquitin ligase that recognizes sugar chains. *Nature* **418**, 438–442 (2002).
8. Yoshida, Y. *et al.* Fbs2 is a new member of the E3 ubiquitin ligase family that recognizes sugar chains. *J. Biol. Chem.* **278**, 43877–43884 (2003).
9. Zheng, N. *et al.* Structure of the Cul1-Rbx1-Skp1-F boxSkp2 SCF ubiquitin ligase complex. *Nature* **416**, 703–709 (2002).
10. Wu, G. *et al.* Structure of a β-TrCP1-Skp1–β-catenin complex: destruction motif binding and lysine specificity of the SCF(β-TrCP1) ubiquitin ligase. *Mol. Cell* **11**, 1445–1456 (2003).
11. Orlicky, S., Tang, X., Willems, A., Tyers, M. & Sicheri, F. Structural basis for phosphodependent substrate selection and orientation by the SCF^{Cdc4} ubiquitin ligase. *Cell* **112**, 243–256 (2003).
12. Schulman, B.A. *et al.* Insights into SCF ubiquitin ligases from the structure of the Skp1-Skp2 complex. *Nature* **408**, 381–386 (2000).
13. Plemper, R.K. & Wolf, D.H. Retrograde protein translocation: ERADication of secretory proteins in health and disease. *Trends Biochem. Sci.* **24**, 266–270 (1999).
14. Fiedler, K. & Simons, K. The role of *N*-glycans in the secretory pathway. *Cell* **81**, 309–312 (1995).
15. Helenius, A. & Aebi, M. Intracellular functions of *N*-linked glycans. *Science* **291**, 2364–2369 (2001).
16. Ellgaard, L., Molinari, M. & Helenius, A. Setting the standards: quality control in the secretory pathway. *Science* **286**, 1882–1888 (1999).
17. Holm, L. & Sander, C. Protein structure comparison by alignment of distance matrices. *J. Mol. Biol.* **233**, 123–138 (1993).
18. Seetharaman, J. *et al.* X-ray crystal structure of the human galectin-3 carbohydrate recognition domain at 2.1-Å resolution. *J. Biol. Chem.* **273**, 13047–13052 (1998).
19. Simpson, P.J. *et al.* The solution structure of the CBM4-2 carbohydrate binding module from a thermostable *Rhodothermus marinus* xylanase. *Biochemistry* **41**, 5712–5719 (2002).
20. Petrescu, A.J., Petrescu, S.M., Dwek, R.A. & Wormald, M.R. A statistical analysis of *N*- and *O*-glycan linkage conformations from crystallographic data. *Glycobiology* **9**, 343–352 (1999)
21. Vyas, N.K. Atomic features of protein–carbohydrate interactions. *Curr. Opin. Struct. Biol.* **1**, 732–740 (1991).
22. Quiocho, F.A. Carbohydrate-binding proteins: tertiary structures and protein–sugar interactions. *Annu. Rev. Biochem.* **55**, 287–315 (1986).
23. Williams, R.L., Greene, S.M. & McPherson, A. The crystal structure of ribonuclease B at 2.5-Å resolution. *J. Biol. Chem.* **262**, 16020–16031 (1987).
24. Leslie, A.G.W. Molecular data processing. *Crystallographic Computing* **5**, 50–61 (1991).
25. Kabsch, W. Evaluation of single-crystal X-ray diffraction data from a position-sensitive detector. *J. Appl. Crystallogr.* **21**, 916–924 (1988).
26. Collaborative Computational Project, Number 4. The CCP4 suite: programs for protein crystallography. *Acta Crystallogr. D* **50**, 760–763 (1994).
27. Wang, B.C. Resolution of phase ambiguity in macromolecular crystallography. *Methods Enzymol.* **115**, 90–112 (1985).
28. Zhang, K.Y.J. & Main P. The use of Sayre's equation with solvent flattening and histogram matching for phase extension and refinement of protein structures. *Acta Crystallogr. A* **46**, 377–381 (1990).
29. Perrakis, A., Morris, R. & Lamzin, V.S. Automated protein model building combined with iterative structure refinement. *Nat. Struct. Biol.* **6**, 458–463 (1999).
30. Jones, T.A., Zou, J.Y., Cowan, S.W. & Kjeldgaard. Improved methods for building protein models in electron density maps and the location of errors in these models. *Acta Crystallogr. A* **47** (Part 2), 110–119 (1991).
31. Murshudov, B.W. Refinement of macromolecular structures by the maximum-likelihood method. *Acta Crystallogr. D* **53**, 240–255 (1997).
32. Navaza, J. An automated package for molecular replacement. *Acta Crystallogr. A* **50**, 157–163 (1994).
33. Kawakami, T. *et al.* NEDD8 recruits E2-ubiquitin to SCF E3 ligase. *EMBO J.* **20**, 4003–4012 (2001).
34. Clore, G.M. & Gronenborn, A.M. Multidimensional heteronuclear nuclear magnetic resonance of proteins. *Methods Enzymol.* **239**, 349–363 (1994).

EMBO reports

scientific report

Parkin binds the Rpn10 subunit of 26S proteasomes through its ubiquitin-like domain

Eri Sakata[1], Yoshiki Yamaguchi[1], Eiji Kurimoto[1], Jun Kikuchi[2], Shigeyuki Yokoyama[2,3], Shingo Yamada[4], Hiroyuki Kawahara[4], Hideyoshi Yokosawa[4], Nobutaka Hattori[5], Yoshikuni Mizuno[5], Keiji Tanaka[6] & Koichi Kato[1,2+]

[1]Department of Structural Biology and Biomolecular Engineering, Graduate School of Pharmaceutical Sciences, Nagoya City University, Nagoya, Japan; [2]Genomic Sciences Centre, RIKEN Yokohama Institute, Yokohama, Japan; [3]Department of Biophysics and Biochemistry, Graduate School of Science, University of Tokyo, Tokyo, Japan; [4]Department of Biochemistry, Graduate School of Pharmaceutical Sciences, Hokkaido University, Sapporo, Japan; [5]Department of Neurology, School of Medicine, Juntendo University, Tokyo, Japan & [6]Department of Molecular Oncology, Tokyo Metropolitan Institute of Medical Science, Tokyo, Japan

Parkin, a product of the causative gene of autosomal-recessive juvenile parkinsonism (AR-JP), is a RING-type E3 ubiquitin ligase and has an amino-terminal ubiquitin-like (Ubl) domain. Although a single mutation that causes an Arg to Pro substitution at position 42 of the Ubl domain (the Arg 42 mutation) has been identified in AR-JP patients, the function of this domain is not clear. In this study, we determined the three-dimensional structure of the Ubl domain of parkin by NMR, in particular by extensive use of backbone ^{15}N-^{1}H residual dipolar-coupling data. Inspection of chemical-shift-perturbation data showed that the parkin Ubl domain binds the Rpn10 subunit of 26S proteasomes via the region of parkin that includes position 42. Our findings suggest that the Arg 42 mutation induces a conformational change in the Rpn10-binding site of Ubl, resulting in impaired proteasomal binding of parkin, which could be the cause of AR-JP.

EMBO reports 4, 301–306 (2003)
doi:10.1038/sj.embor.embor764

INTRODUCTION

Autosomal-recessive juvenile parkinsonism (AR-JP), one of the most common forms of familial Parkinson's disease, is characterized by selective and massive loss of dopaminergic neurons in the substantia nigra of the midbrain and by the absence of Lewy bodies (cytoplasmic inclusion bodies), which consist of aggregates of abnormally accumulated proteins (Yamamura *et al.*, 1973). The causative gene of AR-JP, *parkin*, encodes a 52-kDa protein composed of three parts: the amino-terminal ubiquitin (Ub)-like domain (Ubl), the carboxy-terminal RING-finger box and the linker region, which connects the two domains (Kitada *et al.*, 1998). Recently, parkin was shown to be a RING-type ubiquitin ligase (or E3 protein) that catalyses protein ubiquitylation, leading to proteasome-mediated protein degradation (Imai *et al.*, 2000; Shimura *et al.*, 2000; Zhang *et al.*, 2000). Analysis of *parkin* mutations in AR-JP patients has revealed that the molecular basis of this disease is the loss of parkin E3-enzyme function in the ubiquitin–proteasome pathway, which may result in the accumulation of parkin substrates in neurons (Chung *et al.*, 2001; Imai *et al.*, 2001; Shimura *et al.*, 2001).

The C-terminal RING box serves as a recruiting motif for ubiquitin-conjugating enzymes (E2 enzymes), such as Ubc4, Ubc7, UbcH7 and UbcH8, whereas the functional role of the N-terminal Ubl domain is poorly characterized. The number of identified mutations in the *parkin* gene in patients with early-onset parkinsonism has recently increased (Lücking *et al.*, 2000), and a single mutation that causes an Arg to Pro substitution at amino-acid position 42 of the Ubl domain has been identified in one family of AR-JP patients (Terreni *et al.*, 2001). This mutated parkin protein retains the ability to bind UbcH7, but fails to co-immunoprecipitate ubiquitylated proteins such as *O*-glycosylated α-synuclein (Shimura *et al.*, 2001). These data suggest that the Ubl domain contributes to the recognition of target proteins.

However, accumulating evidence indicates that various proteins with Ubl domains, such as Rad23, Dsk2 and their human homologues (HR23a/b and PLIC1/2, respectively), provide links between 26S proteasomes and the ubiquitylation machinery (Hiyama *et al.*, 1999; Kleijnen *et al.*, 2000; Wilkinson *et al.*, 2001). All of these proteins have Ubl domains at their N termini, and ubiquitin-associated (UBA) domains at their C termini; the Ubl domains are able to interact

[1]Department of Structural Biology and Biomolecular Engineering, Graduate School of Pharmaceutical Sciences, Nagoya City University, 3-1 Tanabe-dori, Mizuho-ku, Nagoya 467-8603, Japan; [2]Genomic Sciences Center, RIKEN Yokohama Institute, 1-7-29 Suehiro-cho, Tsurumi-ku, Yokohama 230-0045, Japan; [3]Department of Biophysics and Biochemistry, Graduate School of Science, University of Tokyo, 7-3-1 Hongo, Bunkyo-ku, Tokyo 113-0033, Japan; [4]Department of Biochemistry, Graduate School of Pharmaceutical Sciences, Hokkaido University, Sapporo 060-0812, Japan; [5]Department of Neurology, School of Medicine, Juntendo University, 2-1-1 Hongo, Bunkyo-ku, Tokyo 113-0033, Japan & [6]Department of Molecular Oncology, Tokyo Metropolitan Institute of Medical Science, 3-18-22 Honkomagome, Bunkyo-ku, Tokyo 113-8613, Japan
+Corresponding author. Tel/Fax: +81 52 836 3447;
E-mail: kkato@phar.nagoya-cu.ac.jp

**Received 29 August 2002; revised 5 December 2002; accepted 17 December 2002
Published online 21 February 2003**

with 26S proteasomes, whereas the UBA domains can bind to polyubiquitin chains (Buchberger, 2002). However, it has been reported that a 50-kDa subunit of human 26S proteasomes, originally called S5a, can bind to polyubiquitin conjugates *in vitro*, and could therefore possibly function as a polyubiquitin-binding subunit (Deveraux *et al.*, 1994). Several S5a homologues (such as Mbp1, Mcb1, Sun1, Pus1, μ-54 and Rpn1) have been identified in various eukaryotes (Kawahara *et al.*, 2000). Here, we call S5a and its homologues 'Rpn10' on the basis of a recent proposal (Finley *et al.*, 1998). Intriguingly, Rpn10 also binds the Ubl domains of HR23a/b and PLIC2 (Hiyama *et al.*, 1999; Walters *et al.*, 2002). Mutagenesis studies have shown that Rpn10 has two highly conserved polyubiquitin-binding sites, PUbS1 and PUbS2, each of which contains five hydrophobic residues forming an alternating pattern of large and small side-chains (Young *et al.*, 1998). In addition, a homologous motif with a similar structure, known as a ubiquitin-interacting motif (UIM), which physically interacts with ubiquitin and/or polyubiquitylated chains, was recently identified in various proteins (Hofmann & Falquet, 2001). NMR studies have shown that the Ubl domains of HR23a and PLIC2 share a highly conserved hydrophobic surface for binding Rpn10 (Walters *et al.*, 2002). In the Ubl domain of parkin, some of the residues corresponding to those in the hydrophobic Rpn10-binding surface are substituted with polar residues. Therefore, one cannot predict whether parkin can bind 26S proteasomes through interaction with the Rpn10 subunit.

In this study, we have determined the three-dimensional (3D) structure of the Ubl domain of parkin by NMR spectroscopy. Based on chemical-shift-perturbation data, we provide evidence that Ubl interacts with Rpn10 using a surface almost identical to the Rpn10-binding surfaces of the Ubl domains of HR23a and PLIC2. The Rpn10-binding site determined in this study includes position 42 of the parkin Ubl domain. We also discuss how these results relate to the molecular cause of AR-JP.

Table 1 | Statistics for NMR structure calculations

Overhauser-effect distance restraints	
Total number	489
Inter-residue	159
Medium range	71
Long range	66
Intra-residue	193
Number of hydrogen bonds	20
Number of residual dipolar-coupling restraints	129
Dihedral-angle restraints	
ϕ	41
ψ	41
Mean r.m.s. deviation of backbone atoms from the average structure (Å)	0.371 ± 0.117
Mean r.m.s. deviation of all heavy atoms from the average structure (Å)	1.025 ± 0.086
Deviation from idealized covalent geometry	
Bonds (Å)	0.005 ± 0.000
Angles (°)	0.684 ± 0.012
Impropers (°)	0.697 ± 0.012
Ramachandran plot (%)	
Residues in most favourable region	69.1
Residues in additionally allowed region	26.5
Residues in generously allowed region	4.4
Residues in disallowed region	0

RESULTS AND DISCUSSION

The solution structure of the parkin Ubl domain

The Ubl domain of parkin, comprising residues 1–76 of the full-length protein, was produced as a recombinant protein in *Escherichia coli*. Preliminary NMR studies revealed that the Ubl domain forms a disulphide-linked dimer, causing a large amount of aggregation during spectral measurement. Therefore, the solution conditions were optimized by adding 10 mM [$^2H_{10}$] dithiothreitol (DTT). However, the concentration of Ubl never exceeded 0.1 mM, even under these reducing conditions. Therefore, we carried out all spectral measurements using the parkin Ubl domain at a concentration of 0.1 mM. Gel-filtration analysis showed that the Ubl domain was monomeric in the solution conditions used (data not shown). Because extensive collection of the inter-proton restraints based on the nuclear Overhauser enhancement spectroscopy (NOESY) spectra was difficult to carry out, due to dilution of the sample solution (approximately 5–10% of the concentration typically used), the structure determination relied heavily on orientational restraints with respect to the NMR magnetic field. We chose two orientational media: bicelle and cetyltriammonium bromide (CTAB)-doped bicelle (see Methods) for measuring the backbone ^{15}N-^1H residual dipolar couplings (RDCs). The NMR data used for structure calculations are summarized in Table 1. A final set of ten structures was selected for 50 restrained molecular dynamics calculations for the Ubl domain, based on agreement with the experimental data and overall structural quality according to the following prerequisites: no nuclear Overhauser effect (NOE) violations >0.5 Å, no torsion angle violation >5° and no RDC violations >2 Hz (over a 0.6 Hz range) (Fig. 1A). The secondary structure of the parkin Ubl domain consists of two α-helices (α1: residues Ile 23–Arg 33; α2: Gln 57–Asp 60) and five β-sheets (β1: Ile 2–Phe 7; β2: His 11–Val 15; β3: Arg 42–Phe 45; β4: Lys 48–Glu 49; β5: Gln 64–Val 70). These are arranged in a typical ubiquitin fold (Fig. 1B and C). The average r.m.s. deviations from the average structure within the secondary structural elements for backbone atoms and for all heavy atoms are 0.371 Å and 1.025 Å, respectively.

Interaction of the parkin Ubl domain with Rpn10

To analyse the interaction of Rpn10 with the Ubl domain of parkin, we used the Rpn10 fragment comprising residues 196–306 ($Rpn10_{196-306}$), which retains both PUbS1 and PUbS2. Figure 2A shows a comparison of the ^1H-^{15}N heteronuclear single-quantum coherence (HSQC) spectra of the uniformly-[^{15}N]-labelled Ubl domain in the presence and absence of $Rpn10_{196-306}$. Twenty-one significantly perturbed amide resonances were observed, whereas the rest of the spectrum remained unchanged, indicating the formation of a specific complex between Ubl and $Rpn10_{196-306}$ (Fig. 2B). The perturbed residues were mapped onto the Ubl domain structure (Fig. 2C). The identified contact-surface comprised the β3 and β4 strands of the parkin Ubl domain and the residues in their spatial proximity, which corresponds with the Rpn10-binding surfaces of the Ubl domains of PLIC2 and HR23a (Walters *et al.*, 2002).

The Rpn10-binding sites of PLIC2 and HR23a have been characterized by the surface clusters of the hydrophobic residues that are bound by basic residues on the molecular surface, whereas the ubiquitin-binding site of Rpn10 seems to be a hydrophobic area bound by acidic residues (Walters *et al.*, 2002). In PLIC2, the hydrophobic cluster comprises residues Ile 75, Ala 77, Ile 80, Val 101 and Ile 102, which correspond to Ile 44, Ala 46, Glu 49, Val 70 and Gln 71, respectively, in parkin. Mutagenesis studies have shown that hydrophobicity at

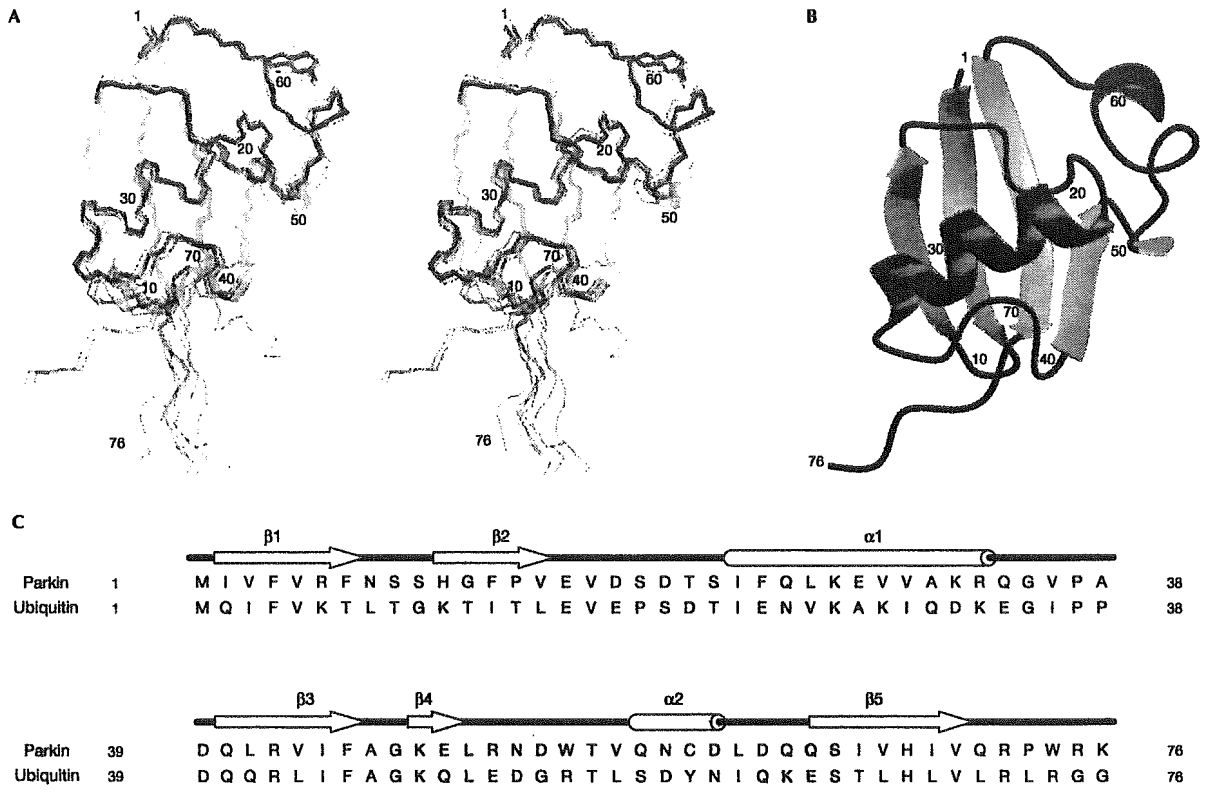

Fig. 1 | The solution structure of the ubiquitin-like (Ubl) domain of parkin. (A) Stereo view of ten converged structures of the parkin Ubl domain. **(B)** Ribbon representation of the average structure. β-strands and α-helices are coloured yellow and pink, respectively, in **(A)** and **(B)**. Numbers in **(A)** and **(B)** indicate amino-acid positions in the Ubl domain sequence. **(C)** Sequence alignment and secondary-structure elements of the parkin Ubl domain and ubiquitin.

amino-acid position 8 in tetraubiquitin is required for its binding to Rpn10 (Beal *et al.*, 1998). Position 8 is occupied by Leu, Pro and Asn in ubiquitin, PLIC2 and parkin, respectively. It should be noted that parkin also has the ability to bind Rpn10, using the surface area corresponding to the hydrophobic cluster of PLIC2 and HR23a, notwithstanding the fact that half of the positions in this cluster are occupied by polar residues in parkin. On the basis of the NMR data from this study, we suggest that interactions between the Rpn10 and Ubl domains are not soley due to the hydrophobic properties of the Ubl domains. It is possible that the relative contributions of the two ubiquitin-binding sites, PUbS1 and PUbS2, are different when binding to different Ubl domains. Indeed, little or no chemical-shift-perturbation was observed for the Ubl domain of parkin after addition of PUbS1 or PUbS2 alone (data not shown). This is in contrast with the finding that the PUbS2 region can interact with the Ubl domain of PLIC2 and HR23a (Walters *et al.*, 2002), suggesting that the modes of the interactions between the Rpn10 and Ubl domains are different, depending on the particular Ubl-domain-containing protein.

Several lines of evidence suggest that E3 proteins associate with 26S proteasomes, thereby recruiting the ubiquitylation machinery (Xie & Varshavsky, 2000; Jäger *et al.*, 2001). The NMR data presented here show the structural basis for the proteasomal binding of E3. Recent studies suggest that the ATPase subunit of 26S proteasomes, not the Rpn10 subunit, is responsible for binding to the polyubiquitin chain (Lam *et al.*, 2002). Taking the data in the present study into consideration, we suggest that parkin and a polyubiquitin-tagged substrate come together on 26S proteasomes to form an efficient assembly line for protein degradation.

Our preliminary experiments revealed that a region of endogenous parkin was co-immunoprecipitated with 26S proteasomes in extracts from Nero2a cells and from mouse brain extracts (data not shown), suggesting that parkin interacts with 26S proteasomes, presumably through the Rpn10 subunit. However, detection of a physical interaction between a glutathione-*S*-transferease (GST)-fused Ubl domain of parkin and FLAG-tagged Rpn10 by co-immunoprecipitation/western blot analysis was unsuccessful, although a clear interaction between HR23a and Rpn10 was seen under the same conditions (see supplementary information online), indicating that the parkin–Rpn10 interaction is weak. Alternatively, it is possible that tagging of parkin and Rpn10 may prevent any interaction between them under *in vitro* conditions. However, in yeast, other proteasome subunits—Rpn1 and/or Rpn2—also bind the ubiquitin-like domain of Rad23 (the yeast

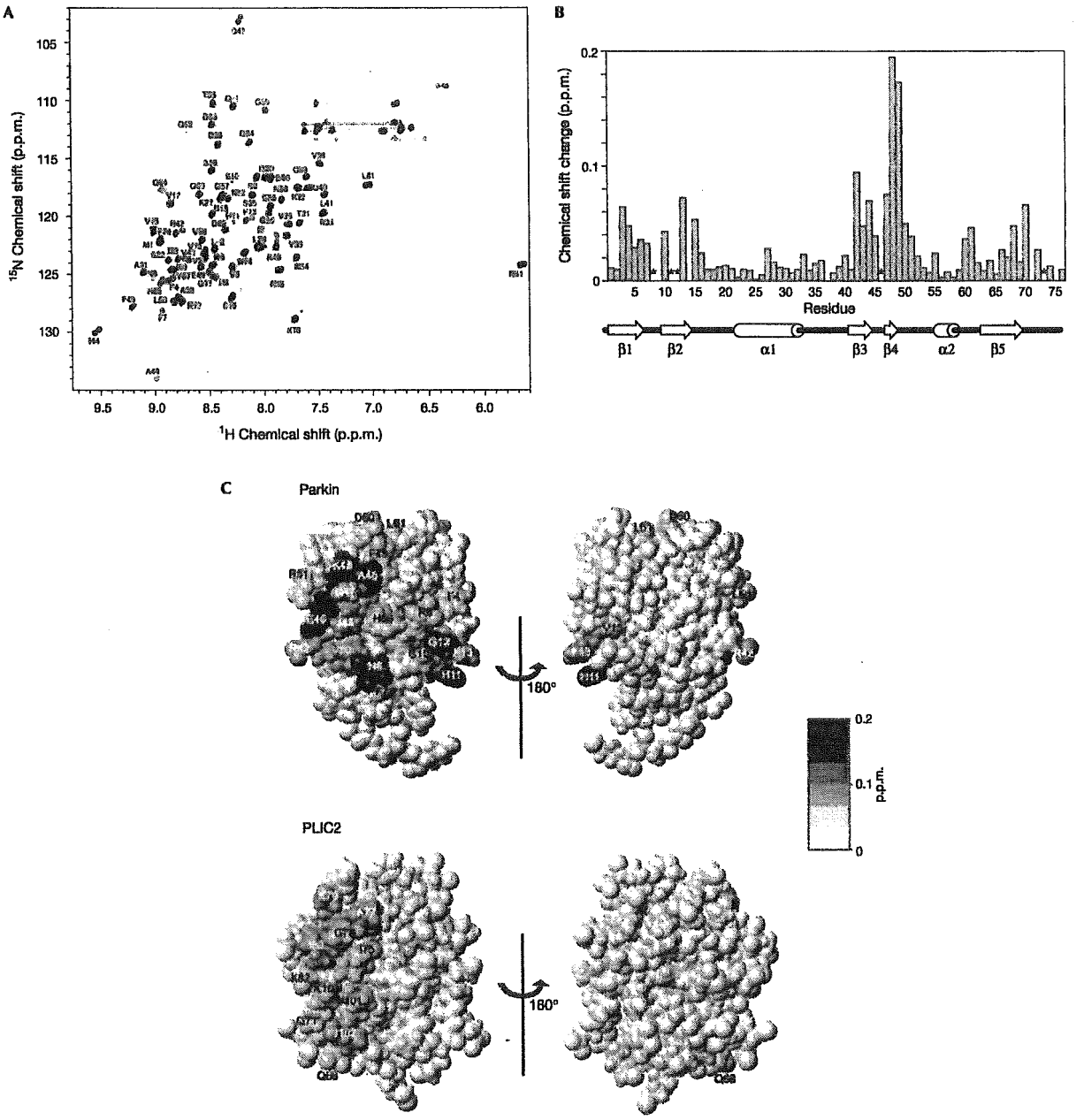

Fig. 2 | Identification of the binding site for Rpn10$_{196-306}$ in the parkin ubiquitin-like (Ubl) domain. (A) ^{1}H-^{15}N heteronuclear single-quantum coherence (HSQC) spectrum of the parkin Ubl domain in the presence (red) and absence (black) of equimolar quantities of Rpn10$_{196-306}$. The peaks labelled with L-2, G-1 and S0 originate from the amino-terminal tag. (B) NMR chemical-shift-perturbation data for the parkin Ubl domain. The data are displayed for each residue according to the equation $(0.2\,\delta_N^2 + \delta_H^2)^{1/2}$, where δ_N and δ_H represent the change in nitrogen and proton chemical shifts on addition of Rpn10$_{196-306}$. Asterisks indicate residues the peaks of which became undetectable due to broadening. Secondary structure elements for the parkin Ubl are shown below the graph. (C) Mapping of the perturbed residues of the Ubl domains of parkin and PLIC2 (Walters *et al.*, 2002) on binding to Rpn10. Residues showing a chemical-shift-perturbation are coloured in red, with the colour gradient indicating the strength of the perturbation. Residues the peaks of which became undetectable on binding to Rpn10 are shown in purple.

homologue of HR23a), when only Rpn1 and/or Rpn2 are assembled into the 26S proteasome complex (Elsasser *et al.*, 2002; Saeki *et al.*, 2002). Therefore, the possibility of an interaction of parkin with Rpn1 and/or Rpn2, as well as with Rpn10, cannot be excluded. It is of note that yeast Rpn10 lacks the PUbS2 sequence (Kawahara *et al.*, 2000) and that the human PUbS2 region, but not the PUbS1 region, can only interact with HR23a (Hiyama *et al.*, 1999). However, it is unclear whether the 26S proteasome subunit(s) that functions as a Ubl-domain acceptor has changed during evolution. The determination of whether both Rpn1/Rpn2 and Rpn10 function redundantly as Ubl-domain acceptors, or whether they have distinct functions, awaits further studies.

SPECULATION

The NMR data presented here indicate that the Arg 42 residue of parkin is located in the Rpn10-binding site. One family of AR-JP patients have a point mutation at position 42 (Terreni *et al.*, 2001), in which Arg is substituted with Pro. It is possible that this mutation induces a significant conformational change in the Rpn10-binding site of the parkin Ubl domain, resulting in impaired proteasomal binding by parkin. Indeed, mutant parkin carrying the Arg-42-Pro mutation was extremely difficult to dissolve at a submillimolar concentration for NMR analysis (data not shown); this insolubility might be associated with loss of the correct functional conformation in the mutant form of parkin. We suggest that this defect hampers the formation of an efficient assembly line for protein degradation, and thereby causes the accumulation of parkin substrates in neurons, leading to Parkinson's disease.

METHODS

Protein expression. The DNA fragment encoding the Ubl domain (amino acids 1–76) of human parkin was cloned into the pGEX-6P-3 vector (Amersham Biosciences) with an N-terminal GST moiety. For expression, the plasmid was cotransformed with the pLysS plasmid (Novagen) into the BL21(DE3)CodonPlus *E. coli* strain (Stratagene). For the production of isotopically labelled protein, cells were grown in M9 minimal media containing [^{15}N]NH_4Cl (1 g l^{-1}) and [u-^{13}C]glucose (2 g l^{-1}). The GST-fusion protein was purified from cell lysates using a glutathione-sepharose column. The fusion protein was cleaved by incubation with 3 units of PreScission protease (Amersham Biosciences) for each milligram of GST-fusion protein for 16 h at 4 °C. GST was removed by the application of the digested products onto a second glutathione-sepharose column. Further purification of the protein was carried out using a Superose12 gel-filtration column (Amersham Biosciences). DNA encoding mouse $Rpn10_{196-306}$ was cloned into the pGEX-6P-1 vector. For expression of $Rpn10_{196-306}$, the plasmid was transformed into the *E. coli* BL21(DE3)CodonPlus strain, and cells were grown in Luria–Bertani media. The expression and purification protocols for $Rpn10_{196-306}$ were generally the same as those used for the parkin Ubl domain.

NMR spectroscopy. NMR samples were prepared at a concentration of 0.1 mM in 90% H_2O/10% ^2H_2O (v/v), 50 mM potassium phosphate buffer, 10 mM [$^2H_{10}$]DTT, pH 6.0. All NMR spectra were recorded at 303 K using Bruker DRX800 or DMX500 spectrometers equipped with 5-mm inverse triple-resonance probes with three-axis gradient coils. Backbone and Cβ resonances were assigned sequentially using the following techniques: two-dimensional (2D) ^{1}H-^{15}N HSQC, constant-time-^{1}H-^{13}C HSQC, and 3D HNCA, HN(CO)CA, HNCO, CBCA(CO)NH and CBCANH spectra. Side-chain and Hα assignments were obtained from HBHA(CO)NH, HBHANH, ^{15}N-edited total-correlation spectroscopy (TOCSY), ^{15}N-edited NOESY, ^{13}C-edited NOESY, HCACO, HCCH-COSY and HCCH-TOCSY spectra. Distance restraints for the parkin Ubl domain were obtained by using ^{15}N-edited NOESY and ^{13}C-edited NOESY spectra. For measurements of residual dipolar couplings, the anisotropic medium used was a nematic-phase liquid-crystalline state, induced by bicelle and cetyltriammonium bromide (CTAB)-doped bicelle (Ottiger & Bax, 1998). The final optimized bicelle concentration for both media was 5% (w/w) for 0.1 mM of the parkin Ubl domain. The 2D ^{1}H-coupled ^{1}H-^{15}N HSQC experiments were used to measure the one-bond ^{15}N-^{1}H scalar coupling ($^1J_{NH}$) values in the isotropic state (in the absence of the liquid-crystalline media) and in the anisotropic media (in the presence of the bicelle or CTAB-doped bicelle). Initial estimates for the axial component of the molecular alignment tensor (*Da*) and the rhombicity (*R*) were obtained from the powder-pattern distribution of the overall ^{15}N-^{1}H RDC ($^1D_{NH}$) values (Clore *et al.*, 1998). These values were then optimized in a stepwise manner, using the calculated solution-structure of the parkin Ubl domain as described previously (Kikuchi *et al.*, 2002). The final values of *Da* and *R* for the parkin Ubl domain were 12 Hz and 0.21, respectively, for the bicelle media, and 18 Hz and 0.42, respectively, for the CTAB-doped bicelle media. Data processing and analysis was carried out using a Silicon Graphics O2 workstation with XWINNMR. The ^{1}H chemical shifts were referenced to external 4,4-dimethyl-4-silapentane-1-sulphonic acid.

Structural determination. Initial calculations were carried out with the NOE-derived inter-proton distance restraints, and with the backbone ϕ and ψ torsion angles restrained by the program TALOS (Cornilescu *et al.*, 1999), and hydrogen-bond restraints in the secondary-structure region. The inter-proton restraints were classified into three categories: 1.8–2.7 Å, 1.8–3.5 Å and 1.8–5.0 Å, corresponding to strong, medium and weak NOE intensities, respectively. The hydrogen-bond restraints (two per hydrogen bond) were set to rNH-O = 1.7–2.3 Å and rN-O = 2.7–3.3 Å, according to the ^{1}H-^{2}H exchange rate for the amide protons, TALOS-based secondary structure identification and the backbone NOE. The RDC-derived restraints were used in the SANI modules (Clore *et al.*, 1998) for performing a direct refinement against the measured dipolar-couplings with the program CNS version 1.1 (Brünger *et al.*, 1998). The calculations were started with extended structures (Nilges *et al.*, 1988), and consisted of a torsion angle space dynamics (TAD) measurement, followed by a Cartesian minimization (Stein *et al.*, 1997). The TAD consisted of 2,000 molecular dynamics steps of 15 picoseconds, carried out at 50,000 K, and a cooling phase (50,000 steps of 5 femtoseconds each) with annealing temperatures from 50,000 K to 0 K. A second TAD cooling-phase, consisting of 10,000 steps of 2 femtoseconds each, was applied, with annealing temperatures from 500 K to 0 K.

The final energy minimization was performed with the following force constants: 1,000 kcal mol^{-1} $Å^{-2}$ for bond lengths, 500 kcal mol^{-1} rad^{-2} for angles and improper torsions (which served to maintain planarity and chirality), 4 kcal mol^{-1} $Å^{-4}$ for the quartic van der Waals repulsion term, 10 kcal mol^{-1} $Å^{-2}$ for the experimental distance restraints, and 0.2 kcal mol^{-1} Hz^{-2} for the $^1D_{NH}$ RDC restraints. The stereochemical quality of the structures of the parkin Ubl domain were assessed using the program PROCHECK-NMR (Laskowski *et al.*, 1996). Graphic figures were generated by the program MOLMOL (Koradi *et al.*, 1996).

Supplementary information is available at *EMBO reports* online (http://www.emboreports.org)

ACKNOWLEDGEMENTS

This work was supported in part by the Yamanouchi Foundation for Research on Metabolic Disorders, by the Naito Foundation and by a Grant-in-Aid for Scientific Research on Priority Areas from the Ministry of Education, Science, Sports and Culture, Japan. The atomic coordinates have been deposited in the RCSB Protein Data Bank (accession code 1IYF).

REFERENCES

Beal, R.E., Toscano-Cantaffa, D., Young, P., Rechsteiner, M. & Pickart, C.M. (1998) The hydrophobic effect contributes to polyubiquitin chain recognition. *Biochemistry*, **37**, 2925–2934.

Brünger, A.T. *et al.* (1998) Crystallography & NMR system: A new software suite for macromolecular structure determination. *Acta Crystallogr. D Biol. Crystallogr.*, **54**, 905–921.

Buchberger, A. (2002) From UBA to UBX: new words in the ubiquitin vocabulary. *Trends Cell Biol.*, **12**, 216–221.

Chung, K.K. *et al.* (2001) Parkin ubiquitinates the alpha-synuclein-interacting protein, synphilin-1: implications for Lewy-body formation in Parkinson disease. *Nature Med.*, **7**, 1144–1150.

Clore, G.M., Gronenborn, A.M. & Bax, A. (1998) A robust method for determining the magnitude of the fully asymmetric alignment tensor of oriented macromolecules in the absence of structural information. *J. Magn. Reson.*, **133**, 216–221.

Cornilescu, G., Delaglio, F. & Bax, A. (1999) Protein backbone angle restraints from searching a database for chemical shift and sequence homology. *J. Biomol. NMR*, **13**, 333–347.

Deveraux, Q., Ustrell, V., Pickart, C. & Rechsteiner, M. (1994) A 26 S protease subunit that binds ubiquitin conjugates. *J. Biol. Chem.*, **269**, 7059–7061.

Elsasser, S. *et al.* (2002) Proteasome subunit Rpn1 binds ubiquitin-like protein domains. *Nature Cell Biol.*, **4**, 725–730.

Finley, D. *et al.* (1998) Unified nomenclature for subunits of the *Saccharomyces cerevisiae* proteasome regulatory particle. *Trends Biochem. Sci.*, **23**, 244–245.

Hiyama, H., Yokoi, M., Masutani, C., Sugasawa, K., Maekawa, T., Tanaka, K., Hoeijmakers, J.H. & Hanaoka, F. (1999) Interaction of hHR23 with S5a. The ubiquitin-like domain of hHR23 mediates interaction with S5a subunit of 26 S proteasome. *J. Biol. Chem.*, **274**, 28019–28025.

Hofmann, K. & Falquet, L. (2001) A ubiquitin-interacting motif conserved in components of the proteasomal and lysosomal protein degradation systems. *Trends Biochem. Sci.*, **26**, 347–350.

Imai, Y., Soda, M. & Takahashi, R. (2000) Parkin suppresses unfolded protein stress-induced cell death through its E3 ubiquitin-protein ligase activity. *J. Biol. Chem.*, **275**, 35661–35664.

Imai, Y., Soda, M., Inoue, H., Hattori, N., Mizuno, Y. & Takahashi, R. (2001) An unfolded putative transmembrane polypeptide, which can lead to endoplasmic reticulum stress, is a substrate of parkin. *Cell*, **105**, 891–902.

Jäger, S., Strayle, J., Heinemeyer, W. & Wolf, D.H. (2001) Cic1, an adaptor protein specifically linking the 26S proteasome to its substrate, the SCF component Cdc4. *EMBO J.*, **20**, 4423–4431.

Kawahara, H. *et al.* (2000) Developmentally regulated, alternative splicing of the Rpn10 gene generates multiple forms of 26S proteasomes. *EMBO J.*, **19**, 4144–4153.

Kikuchi, J., Iwahara, J., Kigawa, T., Murakami, Y., Okazaki, T. & Yokoyama, S. (2002) Solution structure determination of the two DNA-binding domains in the *Schizosaccharomyces pombe* abp1 protein by a combination of dipolar coupling and diffusion anisotropy restraints. *J. Biomol. NMR*, **22**, 333–347.

Kitada, T. *et al.* (1998) Mutations in the parkin gene cause autosomal recessive juvenile parkinsonism. *Nature*, **392**, 605–608.

Kleijnen, M.F., Shih, A.H., Zhou, P., Kumar, S., Soccio, R.E., Kedersha, N.L., Gill, G. & Howley, P.M. (2000) The hPLIC proteins may provide a link between the ubiquitination machinery and the proteasome. *Mol. Cell*, **6**, 409–419.

Koradi, R., Billeter, M. & Wüthrich, K. (1996) MOLMOL: A program for display and analysis of macromolecular structures. *J. Mol. Graph. Model.*, **14**, 51–55.

Lam, Y.A., Lawson, T.G., Velayutham, M., Zweier, J.L. & Pickart, C.M. (2002) A proteasomal ATPase subunit recognizes the polyubiquitin degradation signal. *Nature*, **416**, 763–767.

Laskowski, R.A., Rullmann, J.A., MacArthur, M.W., Kaptein, R. & Thornton, J.M. (1996) AQUA and PROCHECK-NMR: programs for checking the quality of protein structures solved by NMR. *J. Biomol. NMR*, **8**, 477–486.

Lücking, C.B. *et al.* (2000) Association between early-onset Parkinson's disease and mutations in the parkin gene. French Parkinson's Disease Genetics Study Group. *N. Engl. J. Med.*, **342**, 1560–1567.

Nilges, M., Gronenborn, A.M., Brünger, A.T. & Clore, G.M. (1988) Determination of three-dimensional structures of proteins by simulated annealing with interproton distance restraints. Application to crambin, potato carboxypeptidase inhibitor and barley serine proteinase inhibitor 2. *Protein Eng.*, **2**, 27–38.

Ottiger, M. & Bax, A. (1998) Characterization of magnetically oriented phospholipid micelles for measurement of dipolar couplings in macromolecules. *J. Biomol. NMR*, **12**, 261–372.

Saeki, Y., Sone, T., Toh-e, A. & Yokosawa, H. (2002) Identification of ubiquitin-like protein-binding subunits of the 26S proteasome. *Biochem. Biophys. Res. Commun.*, **296**, 813–819.

Shimura, H. *et al.* (2000) Familial Parkinson disease gene product, parkin, is a ubiquitin-protein ligase. *Nature Genet.*, **25**, 302–305.

Shimura, H. *et al.* (2001) Ubiquitination of a new form of alpha-synuclein by parkin from human brain: implications for Parkinson's disease. *Science*, **293**, 263–269.

Stein, E.G., Rice, L.M. & Brünger, A.T. (1997) Torsion-angle molecular dynamics as a new efficient tool for NMR structure calculation. *J. Magn. Reson.*, **124**, 154–164.

Terreni, L., Calabrese, E., Calella, A.M., Forloni, G. & Mariani, C. (2001) New mutation (R42P) of the parkin gene in the ubiquitinlike domain associated with parkinsonism. *Neurology*, **56**, 463–466.

Walters, K.J., Kleijnen, M.F., Goh, A.M., Wagner, G. & Howley, P.M. (2002) Structural studies of the interaction between ubiquitin family proteins and proteasome subunit S5a. *Biochemistry*, **41**, 1767–1777.

Wilkinson, C.R., Seeger, M., Hartmann-Petersen, R., Stone, M., Wallace, M., Semple, C. & Gordon, C. (2001) Proteins containing the UBA domain are able to bind to multi-ubiquitin chains. *Nature Cell Biol.*, **3**, 939–943.

Xie, Y. & Varshavsky, A. (2000) Physical association of ubiquitin ligase and the 26S proteasome. *Proc. Natl Acad. Sci. USA*, **97**, 2497–2502.

Yamamura, Y., Sobue, I., Ando, K., Iida, M. & Yanagi, T. (1973) Paralysis agitans of early onset with marked diurnal fluctuation of symptoms. *Neurology*, **23**, 239–244.

Young, P., Deveraux, Q., Beal, R.E., Pickart, C.M. & Rechsteiner, M. (1998) Characterization of two polyubiquitin binding sites in the 26 S protease subunit 5a. *J. Biol. Chem.*, **273**, 5461–5467.

Zhang, Y., Gao, J., Chung, K.K., Huang, H., Dawson, V.L. & Dawson, T.M. (2000) Parkin functions as an E2-dependent ubiquitin-protein ligase and promotes the degradation of the synaptic vesicle-associated protein, CDCrel-1. *Proc. Natl Acad. Sci. USA*, **97**, 13354–13359.

THE JOURNAL OF BIOLOGICAL CHEMISTRY
Vol. 278, No. 18, Issue of May 2, pp. 16237–16243, 2003
Printed in U.S.A.

Conditional Knockdown of Proteasomes Results in Cell-cycle Arrest and Enhanced Expression of Molecular Chaperones Hsp70 and Hsp40 in Chicken DT40 Cells*

Received for publication, February 6, 2003
Published, JBC Papers in Press, February 19, 2003, DOI 10.1074/jbc.M301331200

Tomoko Tanahashi-Hori‡, Nobuyuki Tanahashi§, Keiji Tanaka‡, and Tomoki Chiba‡¶

From the ‡Department of Molecular Oncology, The Tokyo Metropolitan Institute of Medical Science, 3-18-22 Honkomagome, Bunkyo-ku, Tokyo 113-8613 and the §EPM Project Groups, Osaka R&D Laboratories, Sumitomo Electric Industries Ltd., and New Energy and Industrial Technology Development Organization, Taya-cho 1, Sakae-ku, Yokohama 244-8588, Japan

The 26 S proteasome is an evolutionarily conserved ATP-dependent protease complex that degrades poly-ubiquitinated proteins and plays essential roles in a critical part of cellular regulation. In vertebrates, the roles of the proteasome have been widely studied by use of specific inhibitors, but not genetically. Here, we generated a cell line $Z^{-/-/-}$/Z-HA, in which the expression of the catalytic subunit of the proteasome, Z (β2) could be manipulated. This cell line expresses exogenous Z protein under the control of a tetracycline-repressible promoter in a Z-nullizygous genetic background. Treatment of these cells with doxycycline inhibited Z expression and, hence, the function of the proteasome. The latter resulted in accumulation of poly-ubiquitinated proteins and concomitant induction of molecular chaperones Hsp70 and Hsp40. These results suggest a synergistic role for the proteasome with these molecular chaperones to eliminate misfolded or damaged proteins *in vivo*. Furthermore, knockdown of the proteasome induced apoptotic cell death following cell-cycle arrest at G_2/M phase. Our $Z^{-/-/-}$/Z-HA cell line would be useful for evaluating proteolytic processes catalyzed by the proteasome in many biological events in vertebrate cells.

The 26 S proteasome with a molecular mass of ~2500 kDa consists of the central 20 S protease (catalytic core) and two outer 19 S regulatory particles (alias PA700), functioning as a protein-destroying machine responsible for energy-dependent proteolysis (1, 2). The 20 S proteasome is composed of two copies of 14 different subunits: 7 distinct α and 7 distinct β type subunits. It is a barrel-like particle formed by the axial stacking of four rings made up of two outer α-rings and inner β-rings, being associated in the order of αββα. Three out of seven β-type subunits of each inner ring have catalytically active threonine residues at their N termini, and these active sites reside in a chamber formed by the centers of the abutting β-rings. The eukaryotic 20 S proteasome has at least three different catalytic activities against synthetic peptide substrates; *i.e.* a trypsin-like, chymotrypsin-like, and caspase-like (or peptidylglutamyl-hydrolyzing) activities, that contribute to the hydrolysis of multiple peptide bonds in a single polypeptide by a coordinated mechanism (1, 3, 4).

To date, yeast proteasomal mutants and membrane-permeable inhibitors have been used to determine *in vivo* functions of proteasomes, which have created diverse arrays of evidence on the biological importance of proteasomes such as the cell cycle, immune response, signaling cascades, and protein quality control in various eukaryotes (5, 6). Indeed, budding yeast mutants that lack some peptidase activities have contributed greatly to our understanding of the involvement of proteasomes in the degradation of many unstable key proteins (7), but their application to higher organisms has not been tested. Various substrate-related peptidyl compounds such as MG-132 and Z-L_3VS have been devised as potent inhibitors of proteasomes (8, 9), but caution must be exercised in their use for interpreting proteasome functions, because they inhibit not only proteasomes but also other proteases. In contrast to these compounds, new microbial metabolites, such as lactacystin and eponemycin, were found to induce selective inhibition of proteasomes that do not affect other proteases examined so far (10, 11). However, although these metabolites bind to active threonine residues of proteasomes, the possibility that they inhibit other as-yet-unidentified threonine protease(s) cannot be ruled out completely. Therefore, genetic approaches capable of manipulating proteasomal activities are still required to determine the *in vivo* functions of proteasomes in higher organisms such as vertebrate cells.

For this purpose, we disrupted proteasome subunit Z (formally designated β2) gene (*cpsmb7*) in chicken B cell line DT40 then established $Z^{-/-/-}$/Z-HA cells that express a tetracycline-repressible HA[1]-tagged Z protein (Z-HA). This construct could manipulate proteasome levels in vertebrate cells by repressing the Z-HA by doxycycline (Dox) treatment. Using these cells, we found that reduction of proteasomes caused not only G_2/M arrest during cell-cycle progression but also induction of apoptosis. Moreover, our results surprisingly showed that reduced proteasomes functions induced the expression of major molecular chaperones Hsp70 and Hsp40, suggesting a potential link

* This work was supported in part by a grant-in-aid from the Ministry of Education, Culture, Sports, Science and Technology, Japan. The costs of publication of this article were defrayed in part by the payment of page charges. This article must therefore be hereby marked "*advertisement*" in accordance with 18 U.S.C. Section 1734 solely to indicate this fact.

The nucleotide sequence(s) reported in this paper has been submitted to the GenBank™/EBI Data Bank with accession number(s) AB098728.

¶ To whom correspondence should be addressed. Tel./Fax: 81-3-3823-2237; E-mail: tchiba@rinshoken.or.jp.

[1] The abbreviations used are: HA, hemagglutinin; Bleo, phleomycin; Boc-LRR-AMC, *t*-butyloxycarbonyl-Leu-Arg-Arg-AMC; Bsd, blasticidin; Dox, doxycycline; ODC, ornithine decarboxylase; Puro, puromycin; Suc-LLVY-AMC, succinyl-Leu-Leu-Val-Tyr-7-amino-4-methycoumarine; tTA, tetracycline-controlled transactivator; Z-LLE-AMC, carbobenzoxy-Leu-Leu-Glu-AMC; TdT, terminal deoxytransferase; WST-8, 2-(2-methoxy-4-nitrophenyl)-3-(4-nitrophenyl)-5-(2,4-disulfophenyl)-2H-tetrazolium, monosodium salt; TUNEL, TdT-mediated dUTP-biotin nick end-labeling; ER, endoplasmic reticulum; UPR, unfolded protein response.

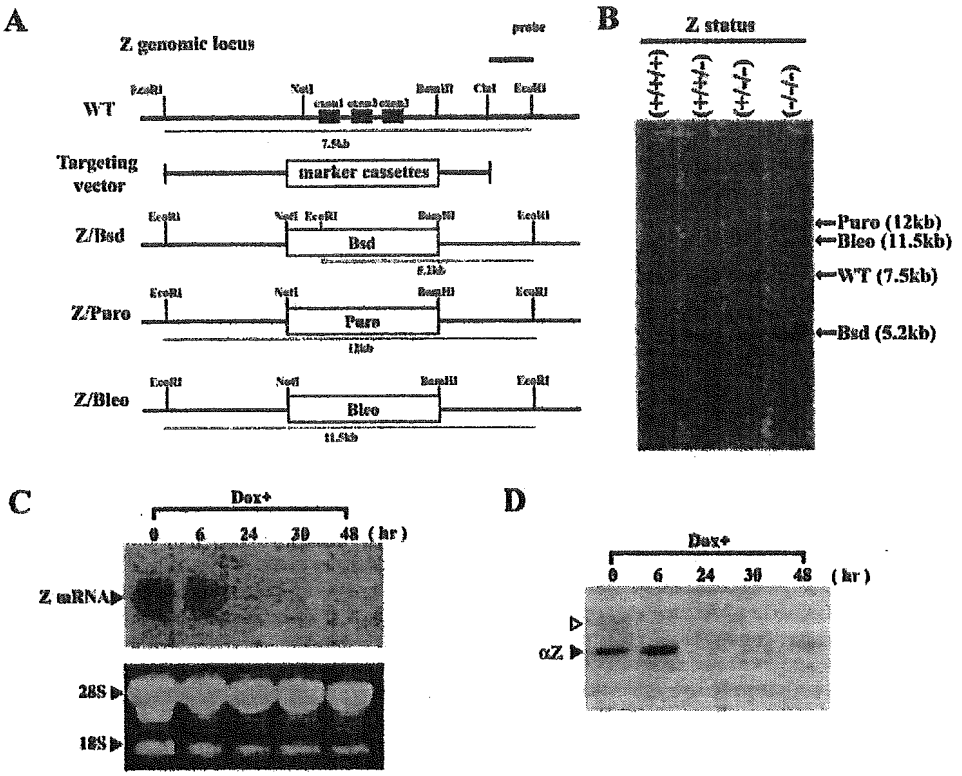

FIG. 1. **Conditional knockdown of proteasome Z subunit in DT40 cells.** *A*, schematic representation of part of Z locus and targeting vectors. Wild-type (*WT*) and targeted alleles (*Z/Bsd*, *Z/Puro*, and *Z/Bleo*) are shown. *B*, genomic Southern blot analysis of wild-type (+/+/+), two heterozygous mutants (+/+/− and +/−/−), and homozygous mutant (−/−/−). Genomic DNAs were digested with *Eco*RI and hybridized with the probe indicated in *A*. *C*, expression of Z-HA mRNA upon Dox treatment. $Z^{-/-/-}$/Z-HA cells were Dox-treated for the indicated times, and total RNAs were subjected to Northern blot analysis. Expression of Z-HA (*top*) and ethidium bromide staining of the total RNAs (*bottom*) are shown. *D*, expression of Z-HA protein upon Dox treatment. Cell extracts (2 μg of protein), obtained from cells treated as in *C*, were Western blotted with anti-chicken Z antibody. The *lower signal* is the mature form (*solid arrowhead*), whereas the *upper signal* corresponds to the precursor form (*open arrowhead*).

between proteasome-mediated proteolysis and stress response for protein homeostasis in the cell.

EXPERIMENTAL PROCEDURES

Plasmid Constructs—Partial chicken Z cDNA was obtained from DT40 cells-derived mRNAs by reverse transcription-PCR method. The primers (5′-GACACGAGGGCGACCGAAGGGATG-3′ and 5′-GCGGCTGCTCAGGAAGTATCCATG-3′) were synthesized based on expressed sequence tag sequence (AJ397675). The full-length cDNA and genomic DNA were obtained by screening chicken muscle cDNA and genomic DNA libraries (Stratagene). The Z targeting vectors were designed by replacing the DNA segment that encompasses exon 1 to exon 3, with drug-resistant cassettes for blasticidin (Bsd), puromycin (Puro), and phleomycin (Bleo). A hemagglutinin (HA) tag was fused to the 3′-end of chicken Z cDNA coding regions by PCR amplifications. HA-tagged chicken Z cDNA (Z-HA) was inserted into the pUHD10–3 vector at the *Eco*RI site and the *Ssp*I site was replaced with the *Hin*dIII site by a *Hin*dIII linker. To construct a tetracycline (tet)-regulatable Z expression vector, tTA-dependent promoter flanked with HA-tagged chicken Z cDNA were recovered from pUHD10–3-Z-HA by digestion with *Hin*dIII and inserted into the *Hin*dIII site of ptTA2-Neo vector (Clontech) that encode tet-repressible tTA (tetR-VP16). The resulting plasmid (ptTA2-Neo-tetZ-HA) expresses Z-HA protein under the control of the tetR-VP16 (12).

Cell Culture and Transfection—DT40 cells were cultured in RPMI1640 medium containing 10% (v/v) fetal bovine serum, 5% (v/v) chicken serum, 10 μM 2-mercaptoethanol, and antibiotics (penicillin and streptomycin) at 39.5 °C under 5% CO_2. Cells were electroporated at 25 microfarads and 550 V (Bio-Rad) as described previously (13). Stable transformants were selected with each drug at the following concentrations: 2.0 mg/ml Geneticin (Sigma), 0.5 μg/ml puromycin (Sigma), 50 μg/ml blasticidin-S (Funakoshi), and 0.3 mg/ml phleomycin (Sigma). Cell viability was assayed by measuring the metabolic activity using tetrazolium salt WST-8 (2-(2-methoxy-4-nitrophenyl)-3-(4-nitrophenyl)-5-(2,4-disulfophenyl)-2H-tetrazolium, monosodium salt, Cell Counting Kit-8, Wako). After incubating the cells with WST-8, the optical density was read as specified by the manufacturer. Dox was used at a concentration of 2 μg/ml for the indicated times.

Antibodies—Anti-chicken Z polyclonal antibody was raised in rabbits using a purified recombinant His-tagged Z protein expressed in *Escherichia coli* BL21. Anti-Hsp70 (MBL), anti-Hsp40 (Stress Gen), anti-actin (Chemicon), anti-Wee1 (Santa Cruz Biotechnology), anti-polyubiquitin (MBL), horseradish peroxidase-conjugated anti-rabbit and anti-mouse IgG antibodies (Amersham Biosciences) were purchased.

Western Blot Analysis—Cells were lysed in 50 mM Tris-HCl (pH 8.0) containing 0.1% TritonX-100 and protease inhibitor mixture (Roche Molecular Biochemicals). Following a brief sonication, the extracts were cleared by centrifugation and subjected to 10–20% SDS-PAGE (14). After transfer onto polyvinylidene difluoride membranes (Millipore), proteins were detected by specific antibodies with the ECL method (Amersham Biosciences). Protein concentration was measured by the method of Bradford with bovine serum albumin as a standard (15).

Southern Blot Analysis—Genomic DNAs were isolated by using a DNeasy tissue kit (Qiagen). Genomic DNA (15 μg) was digested with *Eco*RI, separated in a 0.7% (w/v) agarose gel, and transferred onto a Hybond N^+ nylon membrane (Amersham Biosciences). The membrane was hybridized with ^{32}P-labeled probe (*Cla*I-*Eco*RI fragment indicated in Fig. 1A), washed at high stringency, and then autoradiographed.

Northern Blot Analysis—Total RNAs were isolated by using an RNeasy Mini kit (Qiagen). Approximately 15 μg of total RNAs was separated and transferred onto a Hybond N^+ nylon membrane. The membrane was hybridized with ^{32}P-labeled full-length chicken Z cDNA probe, washed at high stringency, and then autoradiographed.

Glycerol Gradient Fraction—Cells were lysed in 25 mM Tris-HCl (pH 7.5) containing 1 mM dithiothreitol with 2 mM ATP by sonication, and the lysates were centrifuged at 15,000 × *g* for 30 min. The supernatants were subjected to glycerol gradient centrifugation with 10–40% glycerol in the above buffer. After centrifugation at 83,000 × *g* for 22 h using a Beckman SW28 rotor, the gradient was separated into 30 fractions of 1 ml each (16).

Assay of Peptidase Activity—Hydrolysis of the synthetic peptides, succinyl-Leu-Leu-Val-Tyr-7-amino-4-methycoumarine (Suc-LLVY-AMC), *t*-butyloxycarbonyl-Leu-Arg-Arg-AMC (Boc-LRR-AMC), and carbobenzoxy-Leu-Leu-Glu-AMC (Z-LLE-AMC) was measured under the presence or absence of 0.05% SDS as described previously (17). One unit of peptidase activity was defined as the amount that degraded 1 nmol of a given fluorogenic peptide per minute.

Assay of [^{35}S]ODC Degradation Activity—^{35}S-Labeled ornithine decarboxylase (ODC) was produced *in vitro* by translating rat ODC mRNA in rabbit reticulocyte lysates with ^{35}S-labeled Met and Cys (PerkinElmer Life Sciences) and then immunopurified. The degradation of ODC was assayed as described previously (17). In brief, ^{35}S-labeled ODC (3000–4000 cpm) was incubated with antizyme, ATP, and enzyme solution in buffer containing the ATP regeneration system at 37 °C for 1 h. The reaction mixtures were then precipitated with trichloroacetic acid, the radioactivity of the trichloroacetic acid-soluble fraction was measured, and the activity was expressed as a percentage of total ODC radioactivity added.

Flow Cytometric Analysis—Cells were fixed in 70% ethanol in phosphate-buffered saline at 4 °C. Fixed cells were washed in phosphate-buffered saline, incubated with 0.25 mg/ml RNase A at 37 °C, and stained with 10 μg/ml propidium iodide at 4 °C. DNA contents were measured by a flow cytometry and cell cycle profiles were analyzed by the Expo ADC analysis program (Beckman Coulter).

Immunofluorescence and TUNEL Assay—Cells were fixed in 1% paraformaldehyde. For immunofluorescence analysis, anti-HA monoclonal antibody (BAbCO) and Alexa Fluor 594 goat anti-mouse IgG antibody (Molecular Probes) were used. Nuclei were counterstained with TOTO3 (Molecular Probes). Apoptotic cells were detected by TdT-mediated dUTP-biotin nick end-labeling (TUNEL) assay using an Apoptag kit (Intergen). The assay was performed according to instructions provided by the manufacturer. Fluorescence images were obtained using a confocal laser microscope (Zeiss and Bio-Rad).

RESULTS

Genetic Manipulation of Proteasome Function—To examine the cellular roles of proteasomes in vertebrates, we generated a cell line that could genetically manipulate the level of the proteasome subunit that confers a peptidase activity. Chicken B cell line DT40 is advantageous for this purpose, because of its efficient rate of homologous recombination (13). Full-length chicken Z cDNA was obtained by screening a chicken muscle cDNA library using the partial cDNA fragment obtained by reverse transcription-PCR. The full-length chicken Z cDNA deduced a protein of 277 amino acids (accession number AB098728), displaying 57.4% and 83.8% identities with *Saccharomyces cerevisiae* and human, respectively, at the amino acid level. To disrupt the proteasome Z gene (*cpsmb7*), chicken Z genomic DNA was isolated from chicken genomic DNA library, and the targeting vectors were constructed as shown in Fig. 1*A*. The vectors were designed to create a null allele by replacing the DNA segment that encompasses exon 1 to exon 3, which encodes the first 85 amino acids, including the essential catalytic site (threonine 44 in the exon 2), with drug-resistant cassettes. DT40 cells that contain three functional Z genes (*cpsmb7*) were successively transfected with each targeting vector, and the homologously recombined clones were identified by genomic Southern blot (Fig. 1*B*). Because the null mutant was expected to be lethal, we transfected the tet-regulatable Z-HA expression vector (ptTA2-Neo-tetZ-HA vector), in which the expression of Z protein could be shut off by Dox treatment, and isolated their stable transformants after the first allele was disrupted by Bsd construct. The second and third loci were disrupted by Puro and Bleo constructs, respectively. Finally, we obtained the $Z^{-/-/-}$/Z-HA clone that expressed Z-HA in a Z-nullizygous genetic background. The genomic Southern blots of representative clones are shown in Fig. 1*B*. Homologous recombination was identified as appearance of new 5.2-, 12-, and 11.5-kb bands corresponding to the targeted alleles generated by the Bsd, Puro, and Bleo constructs, respectively.

We then tested the effect of Dox treatment on Z-HA expression in $Z^{-/-/-}$/Z-HA cells. Dox treatment of $Z^{-/-/-}$/Z-HA cells reduced the mRNA and protein expression of Z-HA to undetectable levels at 24 h after Dox treatment (Fig. 1, *C* and *D*). Western blot with anti-Z antibody detected both precursor and mature forms of Z-HA. The latter form migrated below the size of the former (Fig. 1*D*). It is known that the catalytic subunits are synthesized as precursor forms and processed into the mature form during the assembly of the 20 S proteasome complex (18). The mature form co-sedimented with the 20 S proteasome, whereas the precursor form was detected in the lighter fraction when the cell extracts were fractionated by glycerol density gradient centrifugation (see Fig. 3, *lower panels*), suggesting that Z-HA is processed and incorporated into the 20 S proteasome.

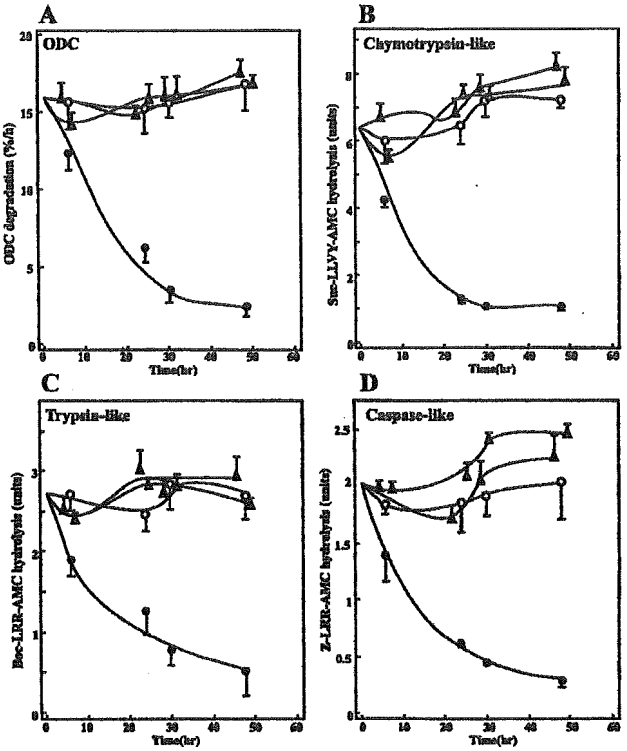

FIG. 2. **Proteasome activities in Dox-treated $Z^{-/-/-}$/Z-HA cells.** Cell extracts (20 μg of protein) were obtained from Dox-treated or untreated cells for indicated times, and peptidase activities were measured against ODC (*A*) and synthetic peptides; *i.e.* a chymotrypsin-like (*B*, Suc-LLVY-AMC), a trypsin-like (*C*, Boc-LRR-AMC), and a caspase-like (*D*, Z-LLE-AMC) activities. *Open circles*, Dox-untreated $Z^{-/-/-}$/Z-HA cells; *solid circles*, Dox-treated $Z^{-/-/-}$/Z-HA cells; *open triangles*, Dox-untreated wild-type cells; *solid triangles*, Dox-treated wild-type cells. Note that a caspase-like activity was assayed in the presence of 0.05% SDS, whereas the chymotrypsin-like and trypsin-like activities were without SDS (for the reason, see Fig. 3, *upper panels*, and text). Data represent the mean ± S.D. values of four independent analyses.

Depletion of Z Subunit Resulted in Loss of Proteasome Activity—Based on yeast studies, Pup1p, which corresponds to Z/β2, is known to confer trypsin-like activity (19, 20). In the next step, we tested whether loss of Z results in specific loss of trypsin-like activity. After Dox treatment, cells were serially collected at the indicated times and cell fractions were prepared. The cell fractions were first tested for their ability to degrade ODC, a proteasome-specific substrate independent of ubiquitination. As shown in Fig. 2*A*, ODC-degrading activities gradually decreased upon Dox treatment. These effects were not seen in Dox-untreated cells or Dox-treated wild-type DT40 cells. Testing for the specificity of peptidase activities showed that not only trypsin-like activity, but also other peptidase

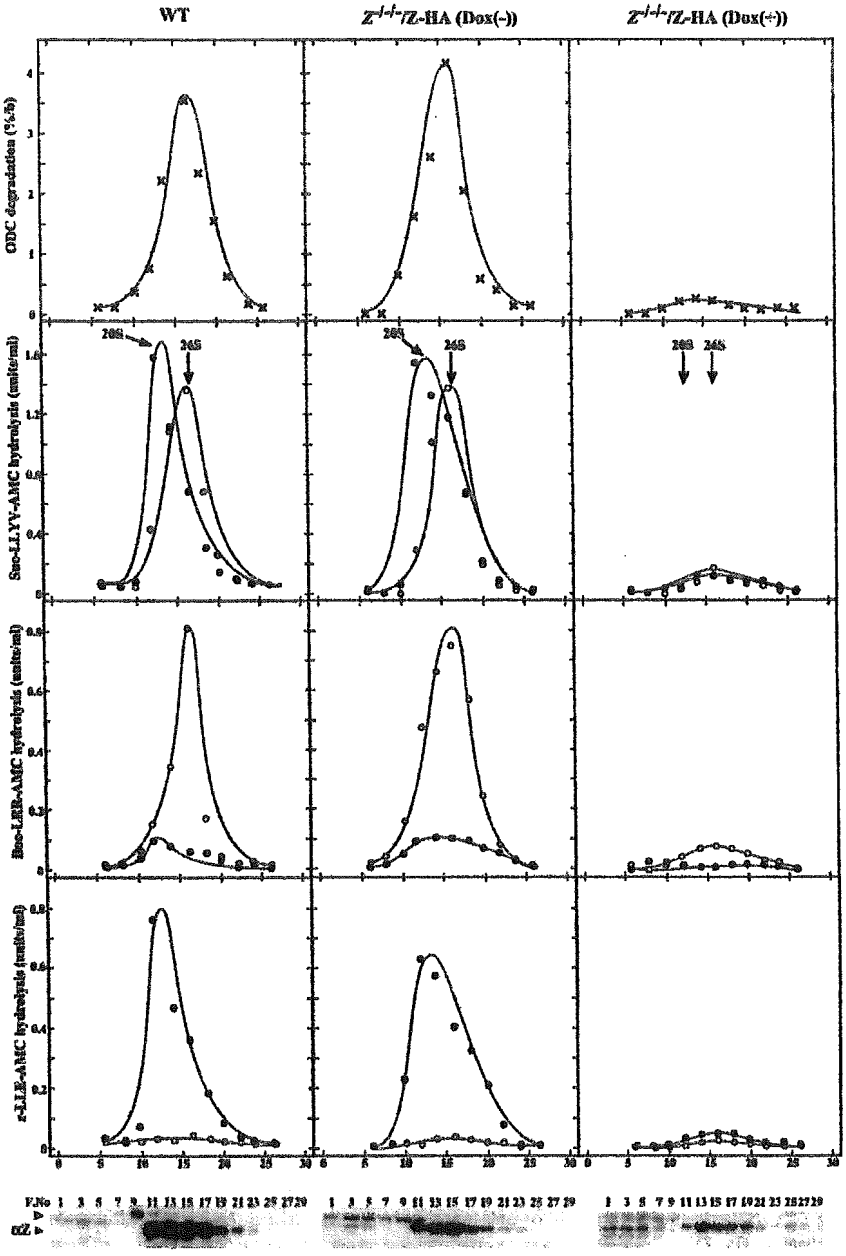

FIG. 3. **Sedimentation velocity analysis of wild-type and $Z^{-/-/-}$/Z-HA cell extracts.** Samples (4 mg of protein) of the wild-type (*WT*) and $Z^{-/-/-}$/Z-HA cells treated with or without Dox for 30 h were fractionated by glycerol density gradient centrifugation (10–40% glycerol from fractions 1 to 30) as described under "Experimental Procedures." After fractionation, aliquots (20 μl) of individual fractions were used for an assay of three peptide hydrolysis with (*solid circles*) or without (*open circles*) 0.05% SDS. The degradation of ^{35}S-ODC (*crosses*) was also assayed. Elution positions of purified 20 and 26 S proteasomes are shown. *Lower panel*, Western blot analysis. Proteins in 200 μl of each fraction were precipitated with acetone, subjected to SDS-PAGE, and stained by Western blot analysis using an anti-chicken Z antibody. *Numbers* correspond to fraction numbers in the *upper panels*. The *solid* and *open arrowheads* point to the mature and precursor forms of Z, respectively, similar to Fig. 1*D*.

chymotrypsin-like and caspase-like activities were reduced (Fig. 2, *B–D*).

To further confirm that these peptidase activities represent proteasome-specific activities, $Z^{-/-/-}$/Z-HA cells were treated with or without Dox for 30 h, and the cell extracts were further fractionated by glycerol density gradient centrifugation and subjected to peptidase assay and Western blot analysis. As shown in Fig. 3 (*upper panels*), in wild-type cells, active enzyme with chymotrypsin-like and trypsin-like activities was sedimented with a sedimentation coefficient of ~26 S, but low activity was found in slowly sedimenting fractions corresponding to the sedimentation position of the purified 20 S proteasome. Addition of 0.05% SDS, which is a potent artificial activator of the latent 20 S proteasome, caused marked enhancement of chymotrypsin-like activity in fractions sedimenting like the 20 S proteasome, as reported previously (16). Note that no obvious caspase-like activity was observed without SDS, but its strong activity could be measured in the presence of 0.05% SDS. ODC-degrading activity as well as these three types of peptidase activities were high and comparable in the Dox-untreated $Z^{-/-/-}$/Z-HA cells at wild-type levels, whereas they were greatly decreased in the Dox-treated $Z^{-/-/-}$/Z-HA cells (Fig. 3, *upper panels*).

Western blot analysis revealed that the mature form of Z protein migrated in the fractions 11–19 with 20–26 S proteasomes (Fig. 3, *lower panels*). The precursor form of Z in wild-type cell extracts migrated at lighter fractions 7–11. These fractions corresponded to 16 S pre-proteasomal particles as reported previously (18). On the other hand, the precursor Z-HA in Dox-untreated $Z^{-/-/-}$/Z-HA cell extracts was recovered in fractions 1–11. The precursor Z-HA observed in fractions 1–5 might be the free form based on its exogenous overexpression. Nonetheless, most mature Z-HA was recovered in the fractions containing sediments of 20–26 S proteasomes, indicating that Z-HA is assembled into these proteasomes. Of note, in the $Z^{-/-/-}$/Z-HA cells with Dox, the mature Z-HA was reduced, and

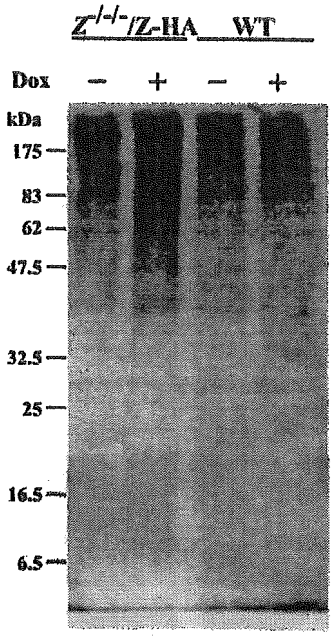

FIG. 4. **Accumulation of poly-ubiquitinated proteins in $Z^{-/-/-}$/Z-HA cells.** The wild-type (*WT*) and $Z^{-/-/-}$/Z-HA cells were treated with (+) or without (−) Dox for 30 h. Cell extracts (10 μg of protein) were subjected to Western blot analysis using an anti-poly-ubiquitin antibody.

precursor Z-HA was not observed in fractions 7–11. In addition, very low mature Z-HA was recovered near top fractions 1–5, which might be generated by disassembly of the 20 S proteasome.

The peptidase activities in fractions of the mature form of Z-HA were high in untreated cells, whereas they were markedly low in Dox-treated cells fractionated in the same manner (Fig. 3, *upper panels*). Taken together, these results suggest that Z-HA is functionally active and that proteasome activity is dependent on the expression of Z-HA. Because not only trypsin-like activity but also other peptidase activities were affected by loss of Z-HA, we concluded that the integral functions of the proteasome are impaired probably due to its inappropriate assembly and/or maintenance of the complex.

Accumulation of Poly-ubiquitinated Proteins Associated with Loss of Z—In the next experiment, we analyzed the levels of cellular poly-ubiquitinated proteins after Z depletion. After wild-type DT40 and $Z^{-/-/-}$/Z-HA cells had been treated with Dox for 30 h, these cell extracts were analyzed by Western blotting using an anti-poly-ubiquitin antibody. As shown in Fig. 4, poly-ubiquitinated proteins considerably increased in crude extracts from the $Z^{-/-/-}$/Z-HA cells by Dox treatment, whereas the pattern of poly-ubiquitinated proteins remained unchanged in wild-type cells, irrespective of Dox treatment. These results suggested that the dysfunction of proteasomes leads to accumulation of poly-ubiquitinated proteins.

Z Subunit Is Essential for Viability—Because most of the proteasome subunit is essential in yeast, we tested the effect of loss of proteasome function on cell viability of $Z^{-/-/-}$/Z-HA cells. For this purpose, $Z^{-/-/-}$/Z-HA cells were treated with Dox for the indicated times and their viability was measured (Fig. 5*A*). Dox-treated $Z^{-/-/-}$/Z-HA cells proliferated in the first 24 h but began to decrease from 30 h of treatment. Flow cytometric analysis of these cells showed their arrest at G_2/M phase (Fig. 5*B*). We next examined the expression of Wee1 kinase, which plays a role in checkpoint mechanism at G_2/M phase (21). Considerable accumulation of Wee1 kinase was noted at 24 h after Dox treatment (Fig. 5*C*). Furthermore, flow cytometry revealed cell death at 30 h after Dox treatment (Fig. 5*B*). To examine whether this was due to apoptosis, we performed TUNEL analysis (Fig. 5*D*). The apoptotic cells had large nuclei and less Z-HA expression. Taken together, these results indicated that loss of Z-HA and proteasomal activities result in cell-cycle arrest at G_2/M phase followed by cell death. It is worth noting that residual Z-HA was present mainly in the cytoplasm as a punctate-like structure and to a lesser extent in the nuclei of Dox-treated cells, whereas it was uniformly present in the cytoplasm and rather abundantly in the nuclei of untreated cells (Fig. 5*D*).

Enhanced Expression of Hsp70 and Hsp40 in Proteasome-defective Cells—It is known that damaged proteins and/or misfolded proteins are rapidly eliminated from the cells by the ubiquitin-proteasome system. Indeed, proteasome inhibitors induce accumulation of such abnormal proteins in the cells and trigger signals that up-regulate the expression of certain molecular chaperones in the cells (22). Given that the expression of proteasomes can be reduced in $Z^{-/-/-}$/Z-HA cells, we next examined whether Z depletion could up-regulate the expressions of major molecular chaperones, Hsp40 and Hsp70 in $Z^{-/-/-}$/Z-HA cells. As shown in Fig. 6 (*lower panels*), Hsp40 and Hsp70 were consistently up-regulated by Z depletion in $Z^{-/-/-}$/Z-HA cells. In contrast, these effects were not observed in Dox-treated wild-type DT40 cells (Fig. 6, *upper panels*). These results suggested that these molecular chaperones are up-regulated upon loss of proteasome function.

DISCUSSION

The proteasome is a multifunctional protease complex and essential for cell viability. We generated $Z^{-/-/-}$/Z-HA cell line in which the expression of proteasome subunit Z could be manipulated by Dox. This cell line expressed Dox-repressible Z protein, tagged with C-terminal HA peptide. The C-terminal HA-tag did not interfere with the wild-type function of Z, because (i) Z-HA complemented the lethality of Z null-phenotype (Fig. 5*A*) and (ii) Z-HA was processed in mature form and incorporated into the proteasome complex (Figs. 1*D* and 3). Depletion of Z-HA resulted in inhibition of three types of proteasomal peptidase activities and ODC-degrading activity (Figs. 2 and 3). Furthermore, considerable accumulation of poly-ubiquitinated cellular proteins was observed *in vivo* (Fig. 4). This is consistent with the fact that cellular poly-ubiquitinated proteins accumulate in the yeast proteasomal temperature-sensitive mutants under restrictive temperature (23). Taken together, these results suggest that the Z subunit is essential for the integrity of proteasome.

The proteasome is the major protease for poly-ubiquitinated proteins and known to degrade many cell-cycle regulators during the cell cycle progression. Most of the yeast proteasome subunit mutants, although not all, exhibit cell-cycle arrest at the G_2/M phase rather than the G_1/S phase (24). Our data also indicate that the major function of the proteasome in cell-cycle regulation is required at the G_2/M phase rather than the G_1/S phase. The essential substrates to be degraded by the proteasome at G_2/M phase were not characterized in this study; however, we observed accumulation of Wee1 kinase in Z-HA knockdown cells (Fig. 5*C*). The Wee1 kinase is known to phosphorylate cyclin-dependent kinase 1 and thus plays a critical role in the checkpoint mechanism by inhibiting cyclin-dependent kinase 1 activity (21). Whether Wee1 kinase is one of the essential substrates or simply accumulates due to cell-cycle arrest at G_2/M phase remains to be elucidated.

The ubiquitin-proteasome system has been implicated in quality control of proteins in the cytosol and endoplasmic reticulum (ER). Accumulation of unfolded proteins in the ER induces the unfolded protein response (UPR), which (i) halts

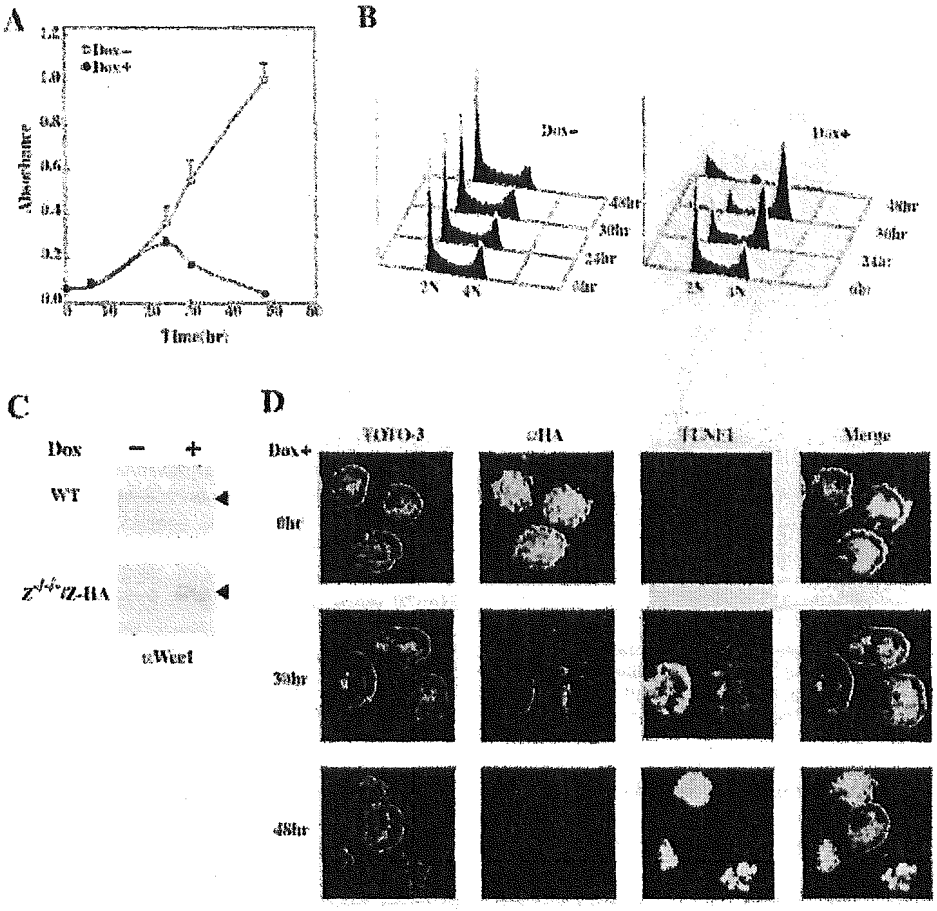

FIG. 5. **The Z subunit is essential for cell viability.** *A*, cell survival after Dox treatment. $Z^{-/-/-}$/Z-HA cells (2×10^4 cells) were cultured in the presence (*solid circles*) or absence (*open circles*) of Dox for indicated times (0, 6, 24, 30, and 48 h), and their viabilities were measured. Data represent the mean ± S.D. values of four independent analyses. *B*, cell cycle analysis. Cells were treated as in *A* and subjected to flow cytometric analyses. *Left panel*, Dox-untreated $Z^{-/-/-}$/Z-HA cells; *right panel*, Dox-treated $Z^{-/-/-}$/Z-HA cells. Displayed data show typical patterns, and essentially similar results were obtained in at least three independent experiments. *C*, increment of Wee1 in Z-depleted cells. The crude extracts (20 μg of protein), prepared from wild-type (*WT*) (*upper panels*) and $Z^{-/-/-}$/Z-HA (*lower panels*) cells that had been cultured with or without Dox for 24 h were immunoblotted with anti-Wee1 antibody. *D*, immunofluorescence analysis. Cells were treated as in *A* for the indicated times (0, 30, and 48 h) and mounted onto slides, fixed, and stained. DNA stain (TOTO-3, *blue*), the expression of Z-HA (αHA, *red*), and apoptotic signals (TUNEL, *green*), in the same cells are shown together with the merged images (*Merge*).

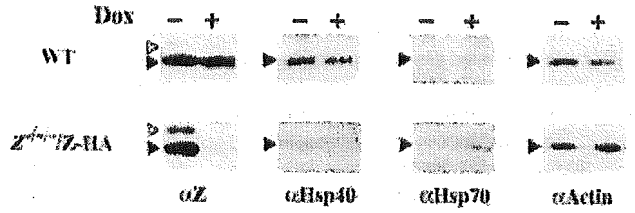

FIG. 6. **Enhanced expression of molecular chaperones Hsp70 and Hsp40 in Dox-treated $Z^{-/-/-}$/Z-HA cells.** Wild-type (*WT*) (*upper panels*) and $Z^{-/-/-}$/Z-HA (*lower panels*) cells were treated with or without Dox for 30 h. Cell extracts (10 μg of protein) were prepared and used for immunoblotting with antibodies against Z, Hsp40, Hsp70, and actin. The *solid arrowheads* indicate the respective proteins, whereas *open arrowheads* show the precursor form of Z.

the translation of newly synthesized proteins, (ii) enhances the expression of molecular chaperones, and (iii) back translocates unfolded protein in the ER to the cytosol for proteasome degradation (25). The last process is called ER-associated protein degradation among the UPR reactions (26). In the present study, our results showed that inhibition of the proteasome enhances the expression of Hsp70 and Hsp40. The latter is known to collaborate with the former for folding newly synthesized and damaged proteins (27). How the cells sense the level of the proteasome and induce these molecular chaperones is unknown at present. However, this process is most likely due to enhanced UPR, because failure of protein degradation results in accumulation of abnormal proteins. Furthermore, the expression of molecular chaperone might be further enhanced following failure of the ER-associated protein degradation pathway.

Ubiquitin and proteasome-dependent protein degradation play essential roles in various biological events as mentioned in the introduction. In this regard, recent studies in the ubiquitin field reveal novel functions for ubiquitin in various biological events such as endocytosis, DNA repair, transcriptional regulation, and kinase activation (28). Whether these events do or do not involve proteasome-dependent degradation remain to be elucidated by genetic means, because proteasome inhibitors are known to inhibit some of the above biological events, such as endocytosis (29). Furthermore, many de-ubiquitinating enzymes that counteract with ubiquitination are vital in the cells (28). Thus, $Z^{-/-/-}$/Z-HA cells could be used as a tool for examining the function of proteasomes in various cellular events that, at least, involve ubiquitination.

Acknowledgments—We thank Y. Yamaguchi-Iwai for providing the parental DT40 cell line, the drug-resistance cassettes, and the pUHD10–3 vector and Y. Murakami for providing ODC and antizyme.

We also thank K. Iwatsuki, T. Yasuda, and all members of the Tanaka laboratory for the advice and technical assistance.

REFERENCES

1. Coux, O., Tanaka, K., and Goldberg, A. L. (1996) *Annu. Rev. Biochem.* **65,** 801–847
2. Baumeister, W., Walz, J., Zuhl, F., and Seemuller, E. (1998) *Cell* **92,** 367–380
3. Groll, M., Ditzel, L., Lowe, J., Stock, D., Bochtler, M., Bartunik, H. D., and Huber, R. (1997) *Nature* **386,** 463–471
4. Unno, M., Mizushima, T., Morimoto, Y., Tomisugi, Y., Tanaka, K., Yasuoka, N., and Tsukihara, T. (2002) *Structure* **10,** 609–618
5. Hershko, A., and Ciechanover, A. (1998) *Annu. Rev. Biochem.* **67,** 425–479
6. Pickart, C. M. (2001) *Annu. Rev. Biochem.* **70,** 503–533
7. Hochstrasser, M. (1997) *Annu. Rev. Genet.* **30,** 405–439
8. Rock, K. L., Gramm, C., Rothstein, L., Clark, K., Stein, R., Dick, L., Hwang, D., and Goldberg, A. L. (1994) *Cell* **78,** 761–771
9. Bogyo, M., McMaster, J. S., Gaczynska, M., Tortorella, D., Goldberg, A. L., and Ploegh, H. (1997) *Proc. Natl. Acad. Sci. U. S. A.* **94,** 6629–6634
10. Fenteany, G., Standaert, R. F., Lane, W. S., Choi, S., Corey, E. J., and Schreiber, S. L. (1995) *Science* **268,** 726–731
11. Kim, K. B., Myung, J., Sin, N., and Crews, C. M. (1999) *Bioorg. Med. Chem. Lett.* **9,** 3335–3340
12. Gossen, M., and Bujard, H. (1992) *Proc. Natl. Acad. Sci. U. S. A.* **89,** 5547–5551
13. Buerstedde, J. M., and Takeda, S. (1991) *Cell* **67,** 179–188
14. Laemmli, U. K. (1970) *Nature* **227,** 680–685
15. Bradford, K. D. (1976) *Anal. Biochem.* **72,** 248–254
16. Tanahashi, N., Murakami, Y., Minami, Y., Shimbara, N., Hendil, K. B., and Tanaka, K. (2000) *J. Biol. Chem.* **275,** 14336–14345
17. Tanaka, K., Yoshimura, T., Kumatori, A., Ichihara, A., Ikai, A., Nishigai, M., Kameyama, K., and Takagi, T. (1988) *J. Biol. Chem.* **263,** 16209–16217
18. Schmidtke, G., Schmidt, M., and Kloetzel, P.-M. (1997) *J. Mol. Biol.* **268,** 95–106
19. Arendt, C. S., and Hochstrasser, M. (1997) *Proc. Natl. Acad. Sci. U. S. A.* **94,** 7156–7161
20. Heinemeyer, W., Fischer, M., Krimmer, T., Stachon, U., and Wolf, D. H. (1997) *J. Biol. Chem.* **272,** 25200–25209
21. Russell, P., and Nurse, P. (1987) *Cell* **49,** 559–567
22. Sherman, M. Y., and Goldberg, A. L. (2001) *Neuron* **29,** 15–32
23. Kominami, K., DeMartino, G. N., Moomaw, C. R., Slaughter, C. A., Shimbara, N., Fujimuro, M., Yokosawa, H., Hisamatsu, H., Tanahashi, N., Shimizu, Y., Tanaka, K., and Toh-e, A. (1995) *EMBO J.* **14,** 3105–3115
24. Ghislain, M., Udvardy, A., and Mann, C. (1993) *Nature* **366,** 358–362
25. Ma, Y., and Hendershot, L. M. (2001) *Cell* **107,** 827–830
26. Plemper, R. K., and Wolf, D. H. (1999) *Trends Biochem. Sci* **24,** 266–270
27. Frydman, J. (2001) *Annu. Rev. Biochem.* **70,** 603–647
28. Weissman, A. M. (2001) *Nat. Rev. Mol. Cell Biol.* **2,** 169–178
29. Longva, K. E., Blystad, F. D., Stang, E., Larsen, A. M., Johannessen, L. E., and Madshus, I. H. (2002) *J. Cell Biol.* **5,** 843–854

THE JOURNAL OF BIOLOGICAL CHEMISTRY
Vol. 278, No. 44, Issue of October 31, pp. 43877–43884, 2003
Printed in U.S.A.

Fbs2 Is a New Member of the E3 Ubiquitin Ligase Family That Recognizes Sugar Chains*

Received for publication, April 21, 2003, and in revised form, August 22, 2003
Published, JBC Papers in Press, August 25, 2003, DOI 10.1074/jbc.M304157200

Yukiko Yoshida‡§¶, Fuminori Tokunaga§‖, Tomoki Chiba‡, Kazuhiro Iwai§‖, Keiji Tanaka‡, and Tadashi Tai‡§

From the ‡Tokyo Metropolitan Institute of Medical Science, Bunkyo-ku, Tokyo 113-8613, Japan, the §Core Research for Engineering, Science, and Technology (CREST), Japan Science and Technology Corporation (JST), Saitama 332-0012, Japan, and the ‖Department of Molecular Cell Biology, Graduate School of Medicine, Osaka City University, Osaka 545-8585, Japan

F-box proteins are substrate recognition components of Skp1-Cullin1-F-box protein-Roc1 (SCF) E3 ubiquitin-protein ligases. We reported previously that Fbs1 (F-box protein that recognizes sugar chains; equivalent to Fbx2 or NFB42) binds specifically to proteins attached with high mannose oligosaccharides and subsequently contributes to elimination of *N*-glycoproteins in cytosol (Yoshida, Y., Chiba, T., Tokunaga, F., Kawasaki, H., Iwai, K., Suzuki, T., Ito, Y., Matsuoka, K., Yoshida, M., Tanaka, K., and Tai, T. (2002) *Nature* 418, 438–442). Here we report the identification of another F-box protein that recognizes *N*-glycan, Fbs2 (called Fbx6b or FBG2 previously). Although the expression of Fbs1 was restricted to the adult brain and testis, the Fbs2 transcript was widely expressed. The Fbs2 protein forms an SCF^{Fbs2} ubiquitin-ligase complex that targets sugar chains in *N*-glycoproteins for ubiquitylation. Only glycoproteins bound to concanavalin A lectin and not to wheat germ agglutinin or *Ricinus communis* agglutinin interacted with Fbs2 in various tissues and cell lines. Pull-down analysis using various oligosaccharides revealed that $Man_{3-9}GlcNAc_2$ glycans were required for efficient Fbs2 binding, whereas modifications of mannose residues by other sugars or deletion of inner GlcNAc reduced Fbs2 binding. Fbs2 interacted with *N*-glycans of T-cell receptor α-subunit (TCRα), a typical substrate of the endoplasmic reticulum-associated degradation (ERAD) pathway, and the forced expression of mutant Fbs2ΔF, which lacks the F-box domain essential for forming the SCF complex, and decrease of endogenous Fbs2 by small interfering RNA led to inhibition of TCRα degradation in cells. Thus, Fbs2 is a novel member of F-box protein family that recognizes *N*-glycans and plays a role in ERAD.

Selective protein degradation by the ubiquitin-proteasome pathway serves as a powerful regulatory mechanism in a wide variety of cellular processes. Ubiquitin conjugation requires the sequential activities of three enzymes or protein complexes called the ubiquitin-activating enzyme (E1),[1] the ubiquitin-conjugating enzyme (E2), and the ubiquitin-protein ligase (E3) (1). In the ubiquitin pathway, E3 plays an important role in the selection of target proteins for degradation, because each distinct E3 usually binds a protein substrate with a degree of selectivity for ubiquitylation. E3s are believed to exist as molecules with a large diversity, presumably in more than hundreds of species, which are classified into many subfamilies. One of the best characterized E3 families is the Skp1-Cullin1-F-box protein-Roc1 (SCF) complex (2). The SCF is composed of a Cullin1/Cdc53, Skp1, Roc1/Rbx1/Hrt1, and one member of a large family of proteins called F-box proteins. F-box proteins typically have a bipartite structure with an N-terminal F box motif consisting of ~40 amino acid residues and a C-terminal region that interacts with the substrate and, thereby, the function of the F-box protein is to trap target proteins (3, 4). However, it remains elusive how E3s accurately recognize target proteins. Accumulating evidence suggests that phosphorylation of target proteins is a prerequisite for their recognition by SCF complexes (1, 2, 4). In addition, it has been shown that proline hydroxylation of the transcription factor hypoxia-induced factor 1α (HIF1α) serves as a signal for ubiquitylation by the SCF-like Cullin2-based VBC ubiquitin-ligase (5, 6). On the other hand, we have reported recently that Fbx2 forms an SCF^{Fbx2} ubiquitin ligase complex that targets sugar chains in *N*-linked glycoproteins for ubiquitylation (7). Thus, Fbx2 is a novel example of F-box proteins that have evolved to recognize protein modifications other than phosphorylation and hydroxylation. *N*-glycosylation acts as a targeting signal to eliminate intracellular glycoproteins by Fbx2-dependent ubiquitylation and subsequent proteasomal degradation.

N-glycosylation of the proteins occurs when newly synthesized proteins enter the endoplasmic reticulum (ER) through the translocation channel "translocon." *N*-glycans play an important role in glycoprotein transport and sorting (8), in particular at the initial step of secretion that occurs in the ER compartment (9, 10). *N*-linked glycoproteins are subjected to "quality control" in which aberrant proteins are distinguished from properly folded proteins and retained in the ER (10). The quality control system includes the calnexin-calreticulin cycle, a unique chaperone system that recognizes $Glc_1Man_{9-6}GlcNAc_2$ and assists refolding of misfolded or unfolded pro-

* This work was supported in part by Grants-in-Aid from the Ministry of Education, Science, and Culture of Japan and the Mizutani Foundation for Glycoscience, Tokyo, Japan. The costs of publication of this article were defrayed in part by the payment of page charges. This article must therefore be hereby marked "*advertisement*" in accordance with 18 U.S.C. Section 1734 solely to indicate this fact.

¶ To whom correspondence should be addressed: Laboratory of Frontier Science, Tokyo Metropolitan Inst. of Medical Science, 3-18-22 Honkomagome, Bunkyo-ku, Tokyo 113-8613, Japan. Tel.: 81-3-3823-2105; Fax: 81-3-3823-2965; E-mail: yyosida@rinshoken.or.jp.

[1] The abbreviations used are: E1, ubiquitin-activating enzyme; E2, ubiquitin-conjugating enzyme; E3, ubiquitin-protein ligase; chitobiose, di-*N*-acetylchitobiose; ConA, concanavalin A; WGA, wheat germ agglutinin; ER, endoplasmic reticulum; ERAD, ER-associated degradation; GST, glutathione *S*-transferase; GTF, GlcNAc-terminated fetuin; HA, hemagglutinin A; RCA, *Ricinus communis*; SCF, Skp1-Cullin1-F-box protein-Roc1; siRNA, small interfering RNA; TBS, Tris-buffered saline; TCRα; T-cell receptor α-subunit; UGGT, UDP-glucose:glycoprotein glucosyltransferase.

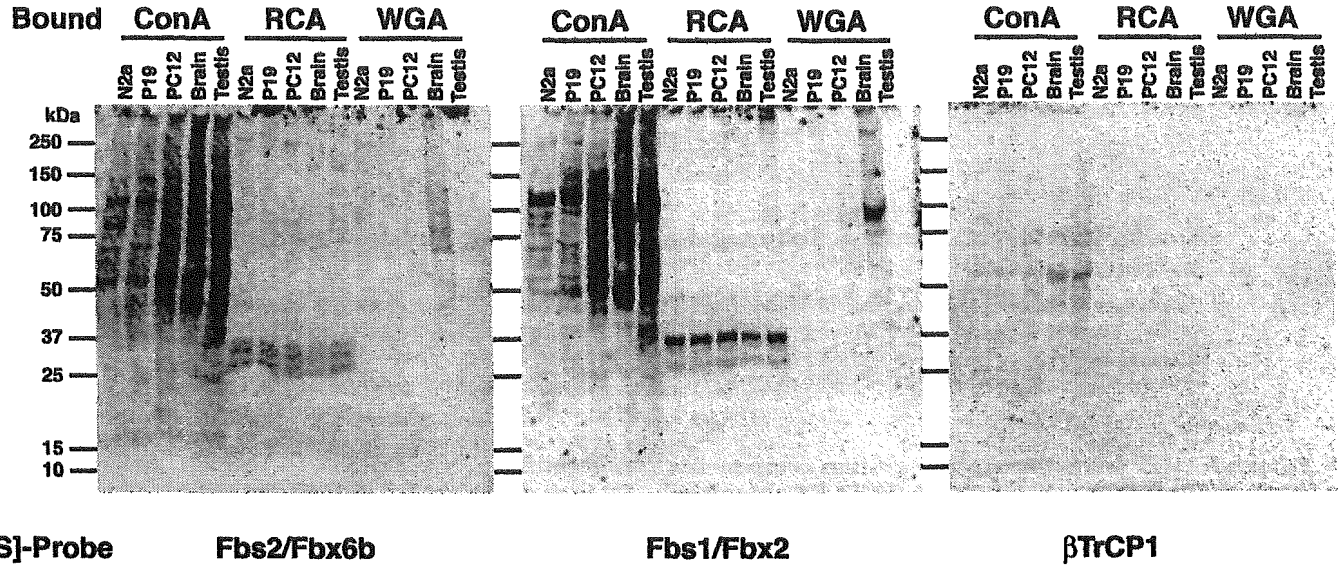

FIG. 1. **Interaction of Fbs2 and Fbs1 with endogenous glycoproteins containing *N*-linked high mannose type oligosaccharides.** Each extract of Neuro2a (*N2a*), P19, PC12 cells, and tissues from adult mice (brain and testis) was incubated with ConA, RCA, or WGA lectin-agarose. The lectin-bound proteins were separated with 4–20% SDS-PAGE and then transferred to membranes that were used for the overlay assay. ^{35}S-labeled Fbs2/Fbx6b ΔF, Fbs1/Fbx2 ΔN-2, and βTrCP1 ΔF were used for the probes.

teins. When the improperly folded or incompletely assembled proteins fail to restore their functional states, they are degraded by the ER-associated degradation (ERAD) system, which involves a retrograde transfer of proteins from the ER to the cytosol followed by degradation by the proteasome (11–13). Precisely how they are selected for ERAD remains unclear, but what is clear is that the trimming of *N*-glycans plays a key role in the selection process. Recent studies have demonstrated that $Man_8GlcNAc_2$ structures serve as part of the signal needed for ERAD and that a lectin for $Man_8GlcNAc_2$ in ER accelerates the turnover rate of the misfolded glycoprotein (14–16). It has been reported that many E3s are involved in the ERAD pathway, such as ER-embedded Hrd1 (17) and Doa10 (18), which have overlapping functions in yeast, and gp78 (19), CHIP (20) and Parkin (21), which ubiquitylate ER membrane proteins such as cystic fibrosis transmembrane conductance regulator (CFTR) and the Pael receptor in mammals. In addition, we have recently identified a novel member of the ERAD-linked E3 family, SCF^{Fbx2}, which participates in ERAD for selective elimination of glycoproteins (7). Misfolding or misassembly might be the general feature of all substrates; however, Fbx2 is expressed mainly in neuronal cells in the adult brain (22). Winston *et al.* (3) and Ilyin *et al.* (23) reported previously that several F-box proteins, including Fbx2, contain a conserved motif F-box-associated (FBA) domain or G-domain (sharing similarity with bacterial protein ApaG) in their C termini.

The present study is an extension of the above mentioned research work and was designed to determine whether these F-box proteins also recognize *N*-glycans. Our results showed that Fbx6b/FBG2 bound several glycoproteins, but other F-box proteins failed to bind any of the glycoproteins tested so far. In considering the results of these functional studies, we renamed Fbx2/FBG1 and Fbx6b/FBG2 Fbs1 (F-box protein that recognizes sugar chains 1) and Fbs2, respectively. We found that Fbs2 is widely distributed in a variety of mouse tissues, differing from the restricted expression of Fbs1. Furthermore, a dominant negative Fbs2 mutant suppressed degradation of a typical ERAD substrate, the T cell receptor α subunit (TCRα). Taken together, we concluded that Fbs2 is a new member of the E3-Fbs subfamily for ubiquitylation of *N*-linked glycoproteins and plays a role in the ERAD pathway.

EXPERIMENTAL PROCEDURES

Materials—Ribonuclease B, fetuin, asialofetuin type II, and thyroglobulin were purchased from Sigma. β-galactosidase (*Streptococcus* 6646K) and β-*N*-acetylhexosaminidase (Jack Bean) were purchased from Seikagaku-Kogyo (Tokyo, Japan), and *N*-glycosidase F was from Roche Applied Science. Affi-Gel 10 and 15 were from Bio-Rad and were used according to the instructions provided by the manufacturer. Di-*N*-acetylchitobiose (chitobiose) was purchased from Seikagaku-Kogyo, $Man_8GlcNAc_2$ was from Glyko (Upper Heyford, UK), $Man_5GlcNAc_1$ was from IsoSep AB, $GlcNAc_2Man_3GlcNAc_2$ (asialo-, agalacto-, tri-antennary complex) and $GlcNAc_2Man_3GlcNAc_2(Fuc_1)$ (asialo-, agalacto-, core-fucosylated bi-antennary complex) were from Ludger (Oxford, UK), and $Man_3GlcNAc_2$, $Man_5GlcNAc_2$, and $Man_5GlcNAc_2$-Asn were purchased from Sigma. $Man_9GlcNAc_2$ was a kind gift from Y. Ito. ConA, RCA, and WGA lectin-agaroses were purchased from Seikagaku-Kogyo.

Isolation of cDNAs Coding for F-box Proteins and Plasmid Construction—The sequences of mouse Fbs2/Fbx6b/FBG2 (accession number AF176526), Fbx17/FBG4 (accession number AF176532), and FBG3 (accession number XM_204068) cDNAs were obtained from the GenBank™ data base. The cDNAs for mouse Fbs2, Fbx17, and FBG3 were amplified by PCR with *Taq* polymerase (Sigma) from mouse kidney cDNA. The PCR primers were as follows: 5′-TCT CTG GGA TCC CCA TGG TCC ACA TCA AGG AG-3′ and 5′-GAG CCT GAG CGG CCG CTA ACG CCT TAG CCT TTG CCA-3′ for Fbs2; 5′-CTG ACC GGA TCC TCA TGG GAG CGC GGC CCT CG-3′ and 5′-ACC TGA AGG CGG CCG CAT CAC ATC ATG GTA GTC C-3′ for Fbx17; and 5′-ACG CCA GGA TCC CAG TAG GCA ACA TCA ACG-3′ and 5′-TGA GGA CTG CGG CCG CTC AGG AGG CAT CAG GGC AG-3′ for FBG3. PCR products were digested with *Bam*HI/*Not*I, subcloned into pBluescriptII SK+, and sequenced. The cDNAs of wild-type or deletion mutants were amplified by PCR with appropriate primers and ligated into *Bam*HI/*Not*I-cut pcDNA3-FLAG or pVL1393-His expression vector. The coding residues of the Fbs2 deletion mutant ΔF were from amino acids 47 to 295.

Overlay Assay—Cultured cells and mouse tissues were homogenized in 10 volumes of TBS (20 mM Tris-HCl, pH 7.5, and 150 mM NaCl) containing 0.5% Nonidet P-40 and protease inhibitor mixture (complete EDTA-free; Roche Applied Science). After centrifugation of the homogenate at 15,000 × *g* for 30 min, each supernatant (15-mg proteins) was incubated with 50 μl of various lectin-agaroses under gentle rotation at 4 °C for 2 h. The agaroses were washed with ice-cold TBS containing 0.5% Nonidet P-40, and bound proteins were boiled with SDS sample buffer. Proteins were separated with SDS-PAGE and blotted onto a membrane (Immobilon, Millipore, Bedford, MA). To prepare the [^{35}S]methionine-Fbs1 and Fbs2 probes, we constructed Fbs1-Metx3 and Fbs2-Metx3 plasmids for Fbs1 (ΔN-2) (7) and Fbs2 (ΔF), respectively, with three additional methionines at the C termini by subcloning them into pcDNA3-FLAG. The TnT Coupled Reticulocyte Lysate System

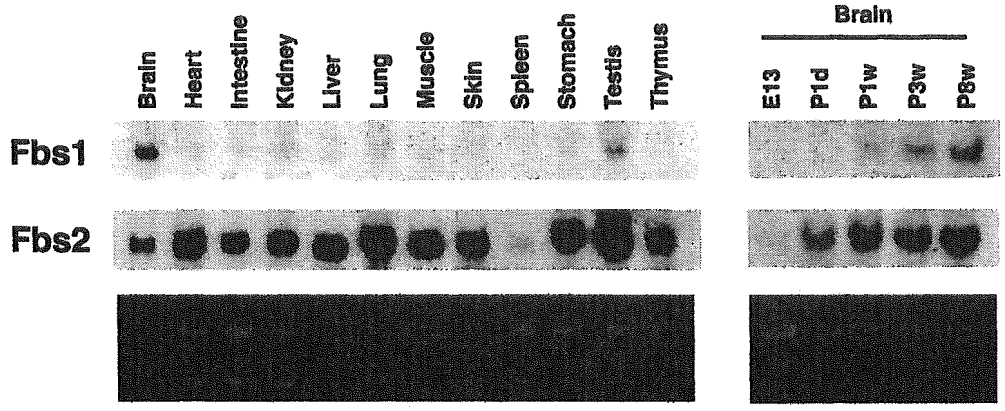

FIG. 2. **Expression of Fbs genes in mouse tissues.** Total RNA was extracted from adult mouse tissues or mice brains at different stages of development. A membrane preloaded with 15 μg of total RNA per lane was hybridized with radiolabeled mouse Fbs1 and Fbs2 cDNAs.

(Promega, Madison, WI) was used for generating [^{35}S]methionine-Fbs1, Fbs2, and βTrCP1. Membranes were blocked by 5% skim milk in TBS, washed, and then incubated with probes in 1% skim milk at 4 °C for 18 h with gentle shaking. Membranes were washed with TBS containing 0.05% Tween 20, air-dried, and analyzed by autoradiography.

Northern Blot Analyses—Tissues from 8-week-old ICR mice were employed for RNA extraction using the guanidine thiocyanate method. 15 μg of total RNA was fractionated on a denaturing formaldehyde-agarose gel (1%) and then transferred onto a nylon membrane (Nytran, Schleicher & Schuell). Northern blots were probed with the full-length Fbs1 or Fbs2 cDNA that had been labeled with [α^{32}P]dCTP. The blots were washed at 65 °C in 0.2× standard saline citrate containing 0.1% SDS and then exposed and analyzed with a Molecular Imager FX (Bio-Rad).

In Vitro Ubiquitylation Assays—Recombinant His-Ubc4 and His-Ubc12, His-NEDD8, and GST-ubiquitin were produced in *Escherichia coli*. Recombinant His-E1 (Uba1), His-APP-BP1/T7-Uba3, and SCF^{Fbs2} (FLAG-Skp1/Cul1-HA/His-Fbs2/T7-Roc1) were produced by baculovirus-infected HiFive or Sf9 insect cells. The SCF^{Fbs2} complex was obtained by simultaneously infecting four baculoviruses. These proteins were affinity-purified by a HiTrap HP column (Amersham Biosciences) as described previously (24).

The methods for preparation of GlcNAc-terminated fetuin (GTF) and deglycosylated fetuin (DGF) were described previously (7). One microgram each of GTF or DGF was incubated in 50 μl of the reaction mixture containing the ATP-regenerating system, 0.5 μg E1, 1 μg of Ubc4 (E2), 2 μg of SCF^{Fbs2}, and 6.5 μg of recombinant GST-ubiquitin in the presence or absence of the NEDD8 system (24) consisting of NEDD8 (10 μg), APP-BP1/T7-Uba3 (0.5 μg), and Ubc12 (0.5 μg) at 30 °C. After terminating the reaction by the addition of 25 μl of 3× SDS-PAGE sample buffer, the proteins in 8 μl of the boiled supernatants were separated with 4–20% SDS-PAGE, and the high molecular mass ubiquitylated proteins were detected by immunoblotting with an anti-fetuin (Chemicon) or anti-GST (Ab-1; Calbiochem, La Jolla, CA) antibody.

Pull-down Assay—Each 2.0 mg of glycoprotein was immobilized to 0.5 ml of Affi-Gel 10 or 15. Each cell extract prepared with TBS containing 0.5% Nonidet P-40 from FLAG-tagged Fbs2 (ΔF) or Fbs1 (ΔN-2)-expressing cells (25 μg) was incubated with 15 μl of various glycoprotein-immobilized beads, and bound proteins were eluted by boiling with SDS sample buffer or incubation with 15 μl of various concentrations of oligosaccharides at room temperature for 10 min. The eluates were separated by spin filtration.

RNA Interference Experiment—Twenty-one nucleotide dsRNAs were prepared by Dharmacon (Lafayette, CO). The siRNA sequences targeting Fbs2 mRNA (GenBank™ accession number NM 018438) corresponded to the coding regions 285–304 (GAGGAUAUGUUUGCAUGGC) and 754–773 (ACAGCAGCAUUGUCGUCAG) relative to the first nucleotide of the start codon. A nonspecific control duplex was purchased from Dharmacon. 293T cells were transfected with siRNA and/or plasmid DNA by the use of LipofectAMINE Plus (Invitrogen). Total RNA was isolated with TRIZOL reagent (Invitrogen). Reverse transcription PCR was performed using total RNA of 293T cells as a template. The 5′ and 3′ primers were 5′-CCTCCTGGCGGGACCTCATCG-3′ and 5′-ACCAGCTGGGACTTGAGGCAC-3′ for Fbs2 and 5′-GAGCTGAACGGGAAGCTCAC-3′ and 5′-ACCACCCTGTTGCTGTAGC-3′ for the glyceroaldehyde-3-phosphate dehydrogenase, respectively.

Metabolic Labeling and Immunoprecipitation—293T cells were transiently transfected with1 μg of the TCRα-HA expression plasmid and 1 μg of the Fbs2 plasmid or pcDNA3. Twenty-four hours after transfection, 293T cells were starved for 30 min in methionine- and cysteine-free Dulbecco's modified Eagle's medium containing 10% dialyzed fetal calf serum. Cells were then labeled for 30 min with 150 μCi of Pro-Mix L-^{35}S *in vitro* cell-labeling mix (Amersham Biosciences) per milliliter. For pulse-chase experiments, cells were washed after labeling and chased with complete Dulbecco's modified Eagle's medium containing 10% fetal calf serum for different lengths of time at 37 °C. In experiments with tunicamycin, cells were treated with 5 μM tunicamycin (Wako Pure Chemical Industries, Osaka, Japan) 2 h prior to and throughout the labeling period. In the experiments of Fbs2 knock-down by siRNA, cells that had been co-transfected with 4.2 μg (300 pmol) of siRNA duplex and 1 μg of the TCRα-HA expression plasmid and cultured for 48 h were metabolically labeled with the cell-labeling mix. After labeling or chase, cells were washed with ice-cold phosphate-buffered saline and lysed with TBS buffer containing 0.1% SDS and 1% Nonidet P-40. In co-immunoprecipitation experiments, TBS buffer containing 1% Triton X-100 was used for lysing. After one cycle of freeze-thaw, cell lysates were cleared by centrifugation, and the supernatants were used for immunoprecipitation. Briefly, the supernatants were precleared with protein A-Sepharose (Amersham Biosciences), mouse monoclonal antibodies, anti-FLAG (M2; Sigma), and anti-HA (HA11, BABCO) were then added, and incubation was performed at 4 °C with rotation. Immune complexes were then incubated with protein A-Sepharose, collected by centrifugation, and washed four times with the lysis buffer. For protein analysis, immune complexes were dissociated by heating in SDS-PAGE sample buffer and loaded onto SDS-PAGE. After drying, gels were exposed, and radioactive band intensity was measured using Molecular Imager FX. All experiments described in this study were approved by the institutional ethics review committee for animal experimentation.

RESULTS

Fbs2 Interacts with High Mannose Oligosaccharide-containing Glycoproteins—We reported recently that Fbs1/Fbx2/NFB42 forms a SCF^{Fbs1} ubiquitin ligase complex that targets *N*-linked high mannose oligosaccharides in glycoproteins for ubiquitylation (7). Fbs1 interacts with substrate glycoproteins through its C-terminal domain, which shows high homology with other F-box proteins (3, 23). To explore the presence of other F-box proteins that recognize *N*-glycans, we isolated mouse cDNA clones that encode F-box proteins homologous to Fbs1 and examined the properties of the proteins with regard to interaction with *N*-linked glycoproteins. The mouse Fbs2/Fbx6b/FBG2, Fbx17/FBG4, and FBG3 cDNA clones obtained by reverse transcription PCR were expressed in 293T cells as FLAG-tagged, full-length F-box proteins, and these cell extracts were incubated with various *N*-linked glycoproteins. Only Fbs2 bound several glycoproteins, whereas the other F-box proteins failed to bind any of the glycoproteins tested (see Fig. 3, and data not shown).

Next, we investigated the interaction of these F-box proteins with oligosaccharides on endogenous proteins by overlay assay. To enrich glycoproteins that were fractionated by their oligo-

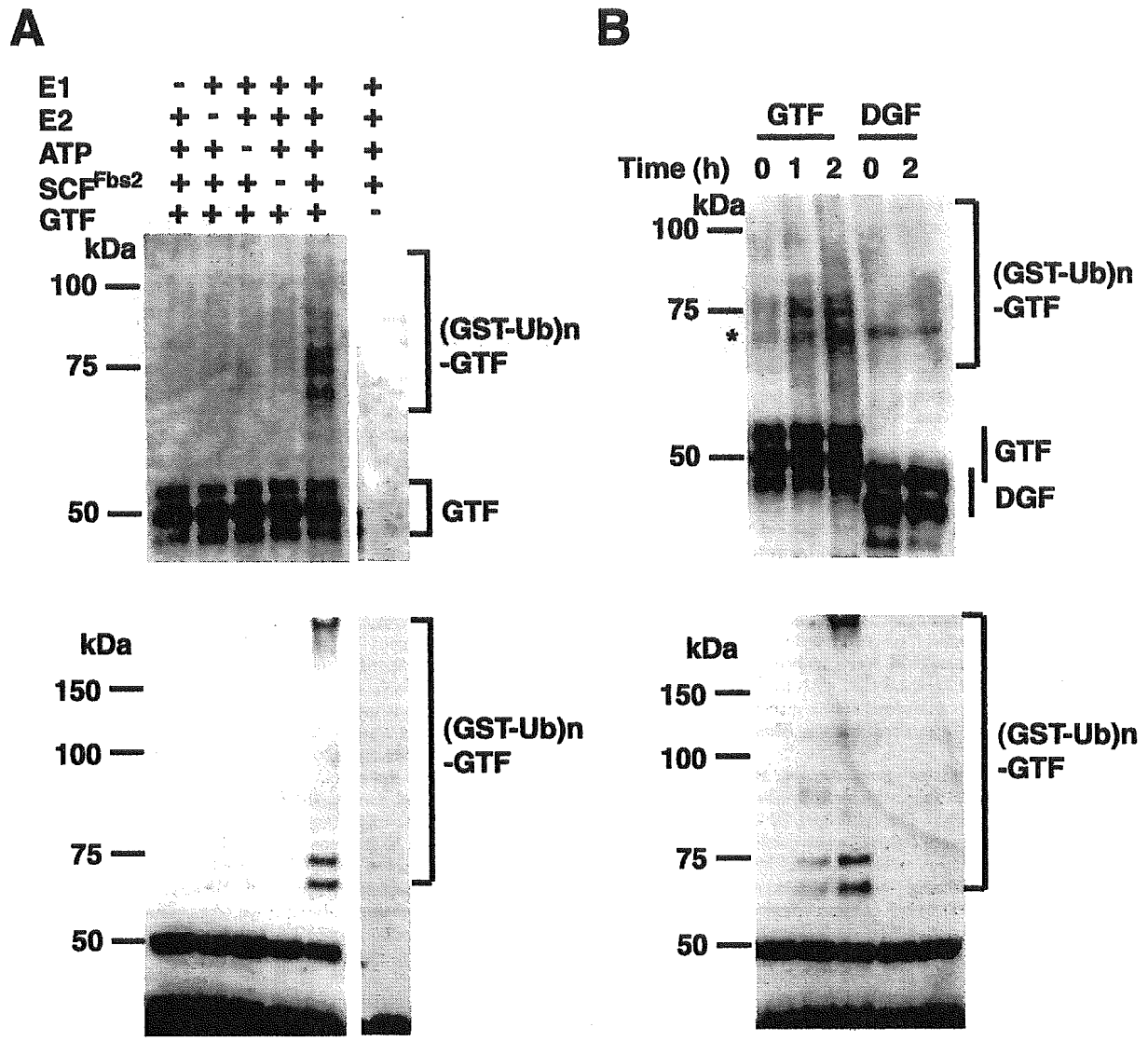

FIG. 3. **SCF^{Fbs2} complex ubiquitylates the *N*-glycosylated substrate *in vitro*.** *A*, *in vitro* ubiquitylation of GTF by the SCF^{Fbs2} E3-ligase system. Ubiquitylation of GTF was confirmed by omission of E1, E2, ATP, E3, or GTF from the reaction mixtures at 30 °C for 2 h. The higher molecular mass-ubiquitylated GTF ((GST-Ub)n-GTF) was detected by immunoblotting with anti-fetuin (*top*) and anti-GST (*bottom*) antibodies. *B*, *N*-linked oligosaccharides are required for ubiquitylation. *In vitro* ubiquitylation was performed with GTF and DGF. *Asterisk*, a nonspecific band detected by anti-fetuin antibody.

saccharide structures, we prepared proteins bound to lectins from the extracts of several cell lines and adult mouse tissues. These glycoproteins were then separated by SDS-PAGE and detected by each ^{35}S-labeled F-box protein. In glycoproteins bound to ConA, a lectin that binds to high mannose oligosaccharides, many protein bands were detected by Fbs1 and Fbs2 probes (Fig. 1). These glycoproteins did not bind to βTrCP1, which is a F-box protein with WD repeats for substrate recognition (1, 2) (Fig. 1). On the other hand, a few proteins reacted with Fbs1 and Fbs2 in the glycoproteins bound to RCA120, a lectin that binds to terminal Galβ1–4GlcNAc or WGA and is specific for terminal GlcNAc or sialic acids (Fig. 1). The broad 75–80-kDa protein band(s) and the 60-kDa protein in the WGA-bound fraction prepared from brain extract seemed to be identical to that bound to ConA. Because many proteins contain several and/or structurally diversified oligosaccharides, these 75–80-kDa and 60-kDa proteins may be modified by high mannose oligosaccharides and complex type glycans. The whole pattern of the protein bands detected by the Fbs2 probe was almost the same as those detected by Fbs1, but the strength of binding activity with Fbs2 seemed to be somewhat weak compared with Fbs1. Any glycoproteins concentrated with ConA, RCA120, and WGA lectins failed to be detected with Fbx17 and FBG3 probes (data not shown). These results suggest that high mannose oligosaccharides are important for the substrate recognition by Fbs2 as well as Fbs1.

Expression of Fbs Genes in Mouse Tissues—Fbs1 is reported to be expressed in the adult rat brain but not in non-neural tissues (22). We compared the expression patterns of Fbs1 and Fbs2 by Northern blot analysis in 12 different mouse tissues. This analysis demonstrated that the Fbs1 transcript of ~1.5 kb mRNA was expressed in the brain and, to a lesser extent, in the testis (Fig. 2). Western blot analysis using Fbs1 polyclonal antiserums confirmed that Fbs1 protein is present only in the brain and testis among the 12 different tissues examined (data not shown). The transcription of Fbs1 appeared in 1-week-old mice, reaching the highest level in the adult brain. On the other hand, an ~1.8-kb transcript of Fbs2 was detected in various tissues, mainly in the heart, intestine, kidney, liver, lung, muscle, stomach, and testis as well as other tissues (brain, skin, spleen, and thymus) with low abundance. Fbs2 expression was not observed in the fetus, but became detectable after birth and increased in the adult brain. Thus, although the